

c.4

SANDIA REPORT

SAND93-2131 • UC-705

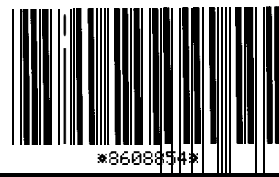
Unlimited Release

Printed September 1993

Prediction of Explosive Cylinder Tests Using Equations of State from the PANDA Code

Gerald 1. Kerley, Tracy L. Christian-Frear

Prepared By
Sandia National Laboratories
Albuquerque, New Mexico 87185 and Livermore, California 94550
for the United States Department of Energy
under Contract DE-AC04-78DP00789



8608834

SANDIA NATIONAL
LABORATORIES
TECHNICAL LIBRARY

Issued by **Sandia** National Laboratories, operated for the United States Department of Energy by **Sandia** Corporation.

NOTICE This report was prepared as an account of work sponsored by an agency of the United States Government. Neither the United States Government nor any agency thereof, nor any of their employees, nor any of their contractors, subcontractors, or their employees, makes any warranty, express or implied, or assumes any legal liability or responsibility for the accuracy, completeness, or usefulness of any information, apparatus, product, or process disclosed, or represents that its use would not infringe privately owned rights. Reference herein to any specific commercial product, process, or service by trade name, trademark, manufacturer, or otherwise, does not necessarily constitute or imply its endorsement, recommendation, or favoring by the United States Government, any agency thereof or any of their contractors or subcontractors. The views and opinions expressed herein do not necessarily state or reflect those of the United States Government, any agency thereof or any of their contractors.

Printed in the United States of America. This report has been reproduced directly from the best available copy.

Available to DOE and DOE contractors from
Office of Scientific and Technical Information
PO Box 62
Oak Ridge, TN 37831

Prices available from (615) 576-8401, FTS 626-8401

Available to the public from
National Technical Information Service
US Department of Commerce
5285 Port Royal Rd
Springfield, VA 22161

NTIS price codes
Printed copy A04
Microfiche copy AO1

SAND93-2131
Unlimited Release
Printed September 28, 1993

Distribution
UC-705

Prediction of Explosive Cylinder Tests Using Equations of State from the PANDA Code

Gerald I. Kerley

Computational Physics and Mechanics Department
Sandia National Laboratories
Albuquerque, NM 87185

Tracy L. Christian-Frear
RE/SPEC Inc.

4775 Indian School Rd., NE, Suite 300
Albuquerque, NM 87110

Abstract

The PANDA code is used to construct tabular equations of state (EOS) for the detonation products of 24 explosives having CHNO compositions. These EOS, together with a reactive burn model, are used in numerical hydrocode calculations of cylinder tests. The predicted detonation properties and cylinder wall velocities are found to give very good agreement with experimental data. Calculations of flat plate acceleration tests for the **HMX-based** explosive LX14 are also made and shown to agree well with the measurements. The effects of the reaction zone on both the cylinder and flat plate tests **are** discussed. For TATB-based explosives, the differences between experiment and theory are consistently larger than for other compositions and may be due to nonideal (finite diameter) behavior.

Contents

Contents	4
List of Figures	5
List of Tables	5
1. Introduction	6
1.1 Background	6
1.2 The Cylinder Test - a Review	6
1.3 Theoretical EOS Model	7
1.4 Scope of Report	8
2. Calculational Model	9
2.1 EOS Tables for Detonation Products	9
2.2 CTH Calculations	10
2.3 Burn Model	11
3. Results	13
3.1 Detonation Properties	13
3.2 Cylinder Tests	15
3.3 Plate Acceleration Tests	21
4. Summary and Conclusions	27
References	28
Appendix A: PANDA Input File for PBX9404	32
Appendix B: CTH Input File for PBX9404 Cylinder Test	34
Appendix C: CTH Input File for LX 14 Plate Acceleration Test	38
Distribution	41

List of Figures

Fig. 1. Results for a 1-in cylinder test of PBX9404	12
Fig. 2. Detonation velocity of TATB-based explosives as a function of reciprocal charge radius	13
Fig. 3. Velocity vs. radius for PBX9404 cylinder test	16
Fig. 4. Velocity and radius vs. time for PBX9404 cylinder test	16
Fig. 5. Results for 1-in and 2-in cylinder tests of LX-14	17
Fig. 6. Cylinder test data for three HMX-based explosives	18
Fig. 7. Cylinder test results for RDX-TNT mixtures	18
Fig. 8. Cylinder test results for HNS at various loading densities	19
Fig. 9. Cylinder test results for PETN and NM	19
Fig. 10. Results for 1-in and 2-in cylinder tests of PBX9502	20
Fig. 11. LX14 flat plate tests #9633 and 9634 of Ref. [21]	23
Fig. 12. Initial acceleration of copper plate for experiments reported in Ref. [21]	24
Fig. 13. Impedance matching diagram for interaction of copper plate with LX14 explosive	24
Fig. 14. LX14 flat plate test #9643 of Ref. [21]	26
Fig. 15. LX14 flat plate test #9526 of Ref. [21]	26

List of Tables

Table 1 Compositions and heats of formation of explosives	9
Table 2 Experimental and calculated detonation properties	14
Table 3 Summary of copper cylinder wall velocity calculations	22

1. Introduction

1.1 Background

The accurate *a priori* prediction of equations of state (EOS) for the detonation products of high explosives (HE) has been one of the principal aims of explosives research for many years. The empirical JWL (Jones-Wilkins-Lee) EOS formula [1], although very popular and useful, does not provide this predictive capability because it must be fit to experimental data for each new explosive composition. Theoretical “chemical” EOS models, on the other hand, have been shown to give reasonable predictions of explosive detonation properties [2]-[9]. Until recently, however, the chemical models did not offer enough accuracy to be satisfactory alternatives to JWL, even after the model parameters had been adjusted to fit experimental data [10].

To be truly viable as a predictive tool, a theoretical model should give accurate results for the following properties:

1. The steady-state detonation velocity, including its dependence upon loading density and systematic variations in chemical composition of the explosive.
2. The pressure and temperature at the Chapman-Jouguet (CJ) state, i.e. the point of complete decomposition at the end of the reaction zone. (These quantities usually cannot be determined as accurately as the detonation velocity [10].)
3. The expansion behavior of the detonation products behind the detonation front, normally studied using cylinder tests and other hydrodynamic experiments [1].
4. The overdriven Hugoniot, i.e. the shock properties of the detonation products compressed above the CJ point [11].

In this report we will consider a chemical model for calculating the EOS of explosive detonation products that was first presented at the Eighth Detonation Symposium [7]. This model is available in the PANDA code [12] and will be referred to here as “the PANDA model.” References [7] and [8] showed that the PANDA model gives very good predictions of the detonation properties and the overdriven Hugoniots for explosives having CHNO compositions. We will show that it also gives good predictions for the expansion behavior by comparing it with cylinder test data for 24 explosives.

1.2 The Cylinder Test - a Review

A cylinder test measures the radial expansion of a stick of explosive that is enclosed in a metal tube and detonated at one end. The most common configuration used at Lawrence Livermore National Laboratory [1][10] employs a 30 cm length of explosive with a 1-in diameter, enclosed in a copper tube of thickness 0.26 cm. The radius of the tube as a function of time is recorded at a distance 21 cm from the point of detonation, using a streak camera. The velocity history of the expanding tube is especially important, because the

velocity is closely related to the energy of the expanding gases. Until recently, the velocity history was determined by differentiation of the radius vs. time curve. The velocity can now be determined more precisely using Fabry-Perot interferometers [10].

Experiments on larger diameter sticks have **also been** carried out to investigate time-dependent effects [1]. The results for most explosives satisfy hydrodynamic **scaling, at least** to within experimental error, showing that the **1-in** test approximates infinite diameter behavior. **In** such cases, it is reasonable to conclude that the cylinder test results depend **only** on the detonation product **EOS**, i.e., that they **are** insensitive to reaction rate effects. **How-**ever, some explosives with long reaction zones do exhibit diameter effects that are indicative of time-dependent behavior.

JWL EOS fits for explosive **detonation products are usually** determined by making hydro-code calculations of the cylinder test **and** adjusting the parameters until satisfactory agreement with measured velocity vs. radius curve is obtained [1] [10]. The fit parameters are usually also constrained to match the experiment detonation velocity and pressure. The test data are normally obtained to **2.5-fold expansion** of the cylinder, thereby defining the EOS to about 7-fold volume expansion. Since the products expand adiabatically, a single cylinder test only measures the **adiabat** through the CJ point for a single initial density. In principle, the detonation product EOS should be capable of predicting the cylinder test results for any initial density. In practice, however, separate JWL fits have to be made for each case. This fact shows that the JWL formula, which assumes a constant specific heat and Grüneisen parameter, gives only an approximate representation of states off the CJ adiabat.

The importance of the cylinder test as a diagnostic tool is illustrated by the fact that theoretical EOS models frequently fail to give satisfactory predictions of the results. Souers and Kury [10] recently compared finite element calculations made using different EOS models with cylinder test data for 19 homogeneous explosives. All three theoretical models considered exhibited significant discrepancies (as high as 20-30% in some cases) with the cylinder test data. The predicted detonation velocities were much better. Hence the ability of a model to predict the **CJ** detonation properties does not guarantee its ability to predict the detonation product expansion.

1.3 Theoretical EOS Model

In the PANDA model, separate EOS tables are first constructed for each of the chemical species that are to be allowed in the detonation products. For CHNO compositions, the **principal** species are: CO_2 , N_2 , H_2O , CO , NO , NH_3 , CH_4 , H_2 , O_2 , HCOOH (formic acid), atomic N, O, and H, and three forms of condensed carbon - graphite, diamond, and liquid carbon. Fluid perturbation theory [13] is used for all species except for solid carbon. Next, the ideal mixing model is used to compute the thermodynamic functions for a mixture of these species, and the composition of the system is determined from assumption of chemical equilibrium. The same library of EOS tables for the chemical species is used for all explosive compositions. Hence the **only** input parameters required by **PANDA** are the chemical formula $\text{C}_w\text{H}_x\text{N}_y\text{O}_z$ and the heat of formation for the unreacted explosive. (The model has not yet been extended to allow elements other than C, H, N, and O.)

The principal conclusions of previous work are as follows.

- The ideal mixing approximation gives Surprisingly accurate results, not **only** for detonation products, but also when compared with Monte Carlo simulations of mixtures [8][14]. As a result, more realistic EOS can be used for complicated chemical species than would be possible with mixture theories based upon simple intermolecular pair potentials.
- Formic acid is a very important reaction product for explosives having a negative oxygen balance, especially for HMX and RDX. The atomic forms of nitrogen and oxygen are also important in some cases.
- A three-phase model of condensed carbon (graphite, diamond, and liquid) is necessary for explaining variations in detonation properties with changes in composition and loading density. In particular, the transition from graphite to diamond in TNT at high densities was first predicted in Ref. [7].
- In addition to giving good *a priori* predictions of detonation velocities, pressures, and temperatures, the model gives very good agreement with Hugoniot for explosives in the overdrive shock region and Hugoniot of non-explosive CHNO compounds at pressures high enough to create dissociation.

1.4 Scope of Report

Hydrocode calculations of cylinder tests were made for 24 explosives for which experimental data were available. Calculations were also made for plate impact tests of LX14.

Various features of the computational model are discussed in Sec. 2- the EOS tables for the detonation products (Sec. 2.1), the hydrocode input (Sec. 2.2), and the burn model used to propagate the detonation wave along the cylinder (Sec. 2.3).

The results are discussed in Sec. 3. The calculated detonation properties, presented in Sec. 3.1, are shown to agree very well with experimental data for all of the explosives considered. For the detonation velocities, which are the most accurately known detonation properties, the predictions are within $\sim 1.5\%$ of the measurements, on the average. The cylinder test results are presented in Sec 3.2. The calculated cylinder wall velocities are shown to agree with the experimental data to within $\sim 2.6\%$, on the average. In Sec. 3.3, it is shown that the model also gives good predictions of the flat plate impact tests for LX14.

2. Calculational Model

2.1 EOS Tables for Detonation Products

EOS tables for the detonation products of the 24 explosives studied were made using the mixture/chemical equilibrium model in the PANDA code (version 2.06) [12]. The explosive compositions and heats of formation, obtained from Refs. [10], [15], and [16], are listed in Table 1. For composites and mixtures, the chemical formula was defined in terms of an arbitrary mass of explosive [15], since only the relative CHNO ratios affect the EOS. Three of the explosives considered (LX-09, PBX9404, and PBX9502) contain small amounts of elements other than C, H, N, and O. These additional elements were ignored in the present work.

TABLE 1: Compositions and heats of formation of explosives.

Explosive ^a	Formula ^b	$\Delta H_f^\circ(298\text{K})$ (MJ/kg)
BTF	C[6]N[6]O[6]	+2.387
Comp B, Grade A (63% RDX/36% TNT)	C[2.03]H[2.64]N[2.18]O[2.67]	+0.0538
Cyclotol, 77/23 (77% RDX/23% TNT)	C[1.75]H[2.59]N[2.38]O[2.69]	+0.145
HMX	C[4]H[8]N[8]O[8]	+0.253 1
HNB	C[6]N[6]O[12]	+0.1887
HNO ₃ #1 (60% HNO ₃ /40% DNB)	C[1.2]H[1.6]N[1.2]O[3.2]	-1.711
HNO ₃ #2 (60% HNO ₃ /30% DNIY/10% RDX)	C[1.0]H[1.6]N[1.3]O[3.3]	-1.676
HNs	C[14]H[6]N[6]O[12]	+0.174
LX09 (93% HMX/4.6% pDNPA/2.4% FEFO)	C[1.43]H[2.74]N[2.59]O[2.72]F[.02]	+0.0838
LX14 (95.5 %HMX/4.5% Es)	C[1.52]H[2.92]N[2.59]O[2.66]	+0.0628
NM	C[1]H[3]N[1]O[2]	-1.849
NNE (39% NM/56% NP/5% ED)	C[2.0]H[5.2]N[1.1]O[1.9]	-1.908
PBX9011 (90% I-IMW/10% Es)	C[1.73]H[3.18]N[2.45]O[2.61]	-0.170
PBX9404 (94% HMX/3% NC/3% CEF)	C[1.40]H[2.75]N[2.57]O[2.69]Cl[.03]P[.01]	+0.0033 1
PBX9501 (95% HMX/2.5% Es/2.5% BDNP)	C[1.47]H[2.86]N[2.60]O[2.69]	+0.0954
PBX9502 (95% TATB/5% Kel-F)	C[2.30]H[2.23]N[2.21]O[2.21]Cl[.038]F[.13]	-0.8715
PETN	C[5]H[8]N[4]O[12]	-1.7031
RX-23-AA (79% HyN/21% Hy)	H[4.6]N[2.6]O[1.7]	-1.824
RX-23-AB (69% HyN/5% Hy/26% H ₂ O)	H[3.2]N[1.2]O[1.6]	-5.415
RX-23-AC (32% HyN/68% Hy)	H[4.1]N[2.1]O[0.4]	+0.1635
TATB	C[6]H[6]N[6]O[6]	-0.5971
TNGU	C[4]H[2]N[8]O[10]	+0.1559
TNM	C[1]N[4]O[8]	+0.276
TNT	C[7]H[5]N[3]O[6]	-0.295

^aThe following abbreviations were used in specifying the compositions for the mixtures:

Es=Estane; Hy=hydrazine; HyN = hydrazine nitrate.

^bElements other than C, H, N, and O were not included in making the EOS tables.

The PANDA input file for PBX9404, which is typical of that used in all cases, is shown in Appendix A. The detonation products were treated as a mixture of 16 chemical species as described in Sec 1.3. EOS tables for these species had previously been constructed and saved on a data file, as described in Ref. [8]. This same file was used for all explosives, so that only the chemical formula $C_wH_xN_yO_z$ and the heat of formation of the unreacted explosive differed from case to case.

The detonation product EOS were tabulated on a rectangular density-temperature grid covering the range from $0.0 \leq \rho \leq 5.0 \text{ g/cm}^3$ and from $10^3 \sim 10^4 \text{ K}$, equally spaced in $\log(\rho)$ and $\log(T)$, along with points at $\rho=0$ and $T=298\text{K}$. For some explosives, extra densities and temperatures were added in the vicinity of the CJ point to improve resolution and give better results for the detonation properties.

2.2 CTH Calculations

Numerical calculations of the cylinder tests were made using the Eulerian code CTH [17]-[20]. The CTH input file for PBX9404, listed in Appendix B, is typical of those used for tests with a 1-in (2.54 cm) diameter and 0.26 cm wall thickness. A 15-cm length of explosive was used in calculations of the 1-in diameter tests. The radial velocity of the cylinder wall was recorded using tracer particles located near the outside of the copper tube at 7.0, 8.0, and 9.0 cm along the axis from the initiation surface. In order to simulate the experimental conditions, the tracers were only allowed to move in the radial direction; their axial positions were held constant using the "FIXED=Y" option. The fact that the tracers gave nearly identical results for the cylinder wall velocity history showed that steady state conditions had been reached at these positions. For calculations of 2-in cylinder tests, an additional length of 2-5 cm was needed to obtain steady state conditions.

Good resolution of the copper cylinder wall motion was obtained using 0.02-cm zones in the radial direction (13 zones across the tube wall). To minimize computing time, 0.05-cm thick zones were used in the axial direction from 5.0 to 10.0 cm (the region encompassing the tracers), with graded zones at the beginning and end of the stick. Note that this zoning scheme leads to cells with a 2.5:1 aspect ratio in the central part of the problem, a condition which can give poor results in Eulerian calculations and is *not* recommended for general use. Nevertheless, the results were found to be satisfactory in this work because of the fact that the axial and radial flows are nearly independent in cylinder tests. To test the zoning approximations, calculations also were made using 1:1 aspect ratios, using both 0.02-cm and 0.05-cm zone sizes. These tests showed that the use of non-square zoning did not cause any appreciable error. The zone size studies show that the zoning used here is more than adequate to match the precision of most of the experimental measurements. However, much finer zoning would be needed to resolve the ringing behavior in the early time motion with the precision that can be obtained using Fabry-Perot interferometry [21].

The CTH calculations of the flat plate experiments [21], which are discussed in Sec. 3.3, required much finer zoning than did the cylinder tests because the copper thicknesses were much smaller. A sample CTH input file for one of the plate tests is listed in Appendix C, and further details are given in Sec. 3.3.

The copper, in both the cylinder and flat plate tests, was treated using the Mie-Grüneisen EOS and the elastic-perfectly plastic model with a yield strength of 0.35 Gpa and Poisson's ratio of 0.35. To test this approximation, a few calculations were also made with more sophisticated constitutive models [43] [44]; the results did not differ appreciably from those obtained with the simpler model.

2.3 Burn Model

Although the cylinder expansion behavior is determined primarily by the detonation product EOS, reaction rate properties, such as the structure of the reaction zone and curvature of the wave front, can also influence the results. In this work the explosives were initiated by a 1.3-cm long "booster" and burned using the history variable reactive bum model (HVRB) [20]. The detonation of the booster was modeled using the JWL EOS and the CTH programmed bum option [19].

In the HVRB model, the EOS for the partially reacted explosive is given by the expressions [20]

$$P(\rho, T, \lambda) = (1 - \lambda) P_i(\rho, T) + \lambda P_f(\rho, T) \quad (1)$$

and

$$E(\rho, T, \lambda) = (1 - \lambda) E_i(\rho, T) + \lambda E_f(\rho, T) . \quad (2)$$

Here P_f and E_f describe the detonation products and are calculated from the tabular EOS discussed in Sec. 2.1. P_i and E_i describe the unreacted explosive and are calculated from the Mie-Grüneisen formula. The extent of reaction λ is given as a function of time t by

$$\lambda(t) = \min(1, \phi^M) , \quad (3)$$

and

$$\phi(t) = \frac{1}{\tau_0} \int_0^t \left(\frac{P - P_i}{P_r} \right)^z d\tau, \quad (4)$$

where the integrand in Eq. (4) is set to zero for $P < P_i$. The constants P_r , z , M , and P_i for each explosive are calibrated from experimental data, and $\tau_0 = 1.0 \mu\text{sec}$. Where possible, the HVRB parameters used in the cylinder tests calculations were determined by calibrating the model to wedge test data [15] [16], as described in Ref. [20]. For explosives where no wedge tests were available, the parameters were estimated from other initiation data. These calibrations will be discussed in separate reports.

In order to evaluate the importance of reaction rate effects on the numerical results, calculations of a 1-in cylinder test of PBX9404 were made using the JWL EOS with three different bum models. The results are compared with one another and with experimental data [16] [22] in Fig. 1. During the early part of the expansion, the calculation using the HVRB

model (solid line) gives higher expansion velocities than the one using programmed burn (dotted line). The difference between the two models decreases at later times, although the HVRB velocity continues to be about 1% higher out to an expansion of 2.0 cm.

The differences are due, at least in part, to reaction zone effects. The von Neumann spike, which appears only in the HVRB calculation, gives a somewhat higher initial push to the copper tube. A calculation using the CJ volume burn (CJVB) model [20] is also shown in Fig. 1 (dashed line). The CJVB parameters used here were selected so that the detonation wave had no reaction zone; consequently, the results are close to those for programmed burn.

The above results tend to support the usual assumption that the principal features of the cylinder wall motion are determined by the detonation product EOS. However, they show that reaction rate effects do influence the early time behavior and can increase the overall velocity by as much as 1%, even at later times. The reactive burn model was much more important in calculations of the flat plate experiments than in the cylinder tests, because the copper thicknesses were so much smaller. This problem is discussed in Sec. 3.3.

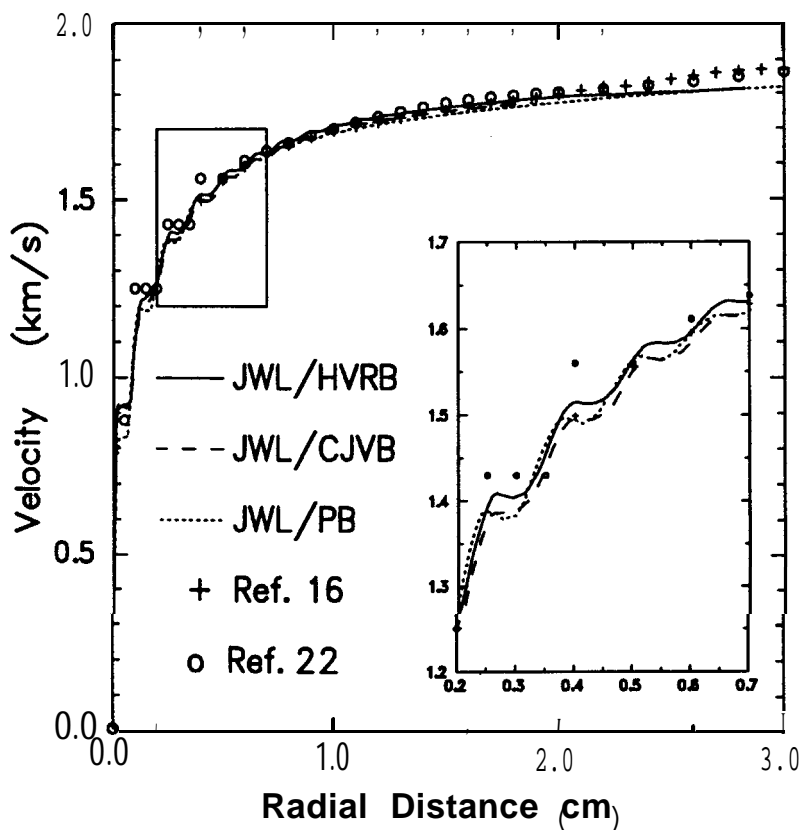


Fig. 1. Results for a 1-in cylinder test of PBX9404. The JWL EOS was used for the detonation products, and the detonation wave was propagated using programmed burn (PB), CJ volume burn (CJVB), and history variable reactive burn (HVRB). The inset figure gives an enlarged view of the region marked by the square. The discrete points are experimental data, as marked.

3. Results

3.1 Detonation Properties

Table 2 gives the experimental and calculated detonation velocities, pressures, and temperatures for the 24 explosives considered in this work. The model gives especially good agreement with the experimental detonation velocities, the most accurately measured quantities. When the results for TATB and PBX9502 are excluded, the average **difference** between the calculated and experimental values is only -0.1%, with a standard deviation of 1.4%, which is comparable to the scatter observed in the experimental measurements.

As previously noted in Ref. [7], the calculated detonation velocities for **TATB-based** explosives are higher than the experimental values by about 5%. In Sec. 3.2 it is shown that a comparable discrepancy is also obtained for the cylinder wall expansion velocities. These differences are well outside those obtained for the other explosives and are not yet fully understood. However, some of the discrepancy is undoubtedly due to nonideal behavior. The measured detonation velocity for 95% **TATB/5% Kel-F** [23][24] is shown as a function of the reciprocal charge radius in Fig. 2. The curve is concave upward at large radii, and the ideal (infinite diameter) value has not been attained even for charge diameters as large as 13 cm. This behavior is different from that seen in other explosives [23], and the infinite diameter value cannot be obtained accurately by the usual extrapolation methods. Therefore, the ideal detonation velocities of **TATB** and for PBX9502 must be higher than the values given in Table 2, i.e. closer to the model predictions.

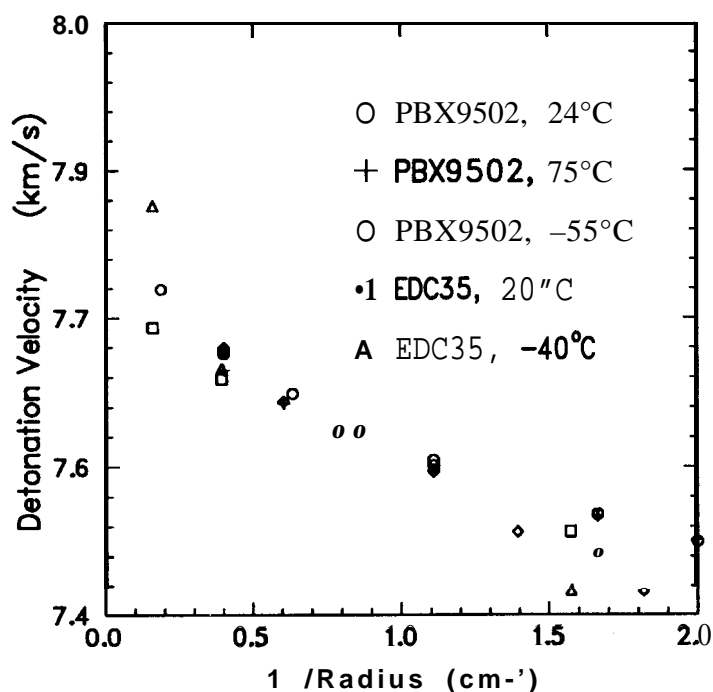


Fig. 2. Detonation velocity of **TATB-based** explosives as a function of reciprocal charge radius; PBX9502 - [23], EDC35 - [24].

TABLE 2: Experimental and calculated detonation properties.

Explosive	Initial Density (g/cm ³)	-----Detonation Properties -----						Refs.
		DC, (km/s)		P _{CJ} (GPa)		T _{CJ} (K)		
		expt.	calc.	expt.	calc.	expt.	calc.	
BTF	1.860	8.49	8.54	36.0	31.4		4480.	[15]
Comp B (Gr. A)	1.720	7.99	7.85	29.5	27.4		3620.	[15]
Cyclotol (77/23)	1.743	8.25	8.18	31.3	29.0		3740.	[16]
HMX	1.891	9.11	9.10	39.0	38.6		3660.	[16][26]
HMX	1.630	8.08	8.06	27.5	27.7	4300.	3950.	[16][26][35]
HMX	1.200	6.59	6.73	15.0	15.3		4330.	[16][26]
HNB	1.965	9.34	9.26	42.5	38.5		5080.	[10]
HNO ₃ #1	1.542	7.23	7.44	21.0	20.4		4620.	[10]
HNO ₃ #2	1.560	7.26	7.37	20.5	19.5		4160.	[10]
HNS	1.681	7.08	7.00	23.0	23.5		3700.	[10][27]
HNS	1.402	6.34	6.23	16.0	16.2		3960.	[10][27]
HNS	1.001	5.10	5.18	7.2	7.18		3830.	[10][27]
LX09	1.840	8.81	8.81	37.7	35.0		3680.	[15]
LX14	1.835	8.83	8.75	37.0	33.8		3580.	[15]
NM	1.130	6.21	6.22	13.4	11.8	3470.	3570.	[28][29][35]
NNE	1.034	5.31	5.38	9.0	7.57		2720.	[10]
PBX9011	1.770	8.50	8.33	29.8	29.4		3420.	[16]
PBX9404	1.846	8.78	8.84	35.6	35.2		3630.	[28][29]
PBX9501	1.832	8.80	8.77		34.0		3640.	[28]
PBX9502	1.890	>7.73 ^a	8.10	28.9	26.4		2730.	[23][29]
PETN	1.763	8.27	8.29	31.5	30.1	4200.	4200.	[30][33]
PETN	1.620	7.85	7.78	26.0	25.4	4400.	4380.	[30][35]
PETN	1.510	7.47	7.40	21.9	21.5		4480.	[30]
PETN	1.230	6.46	6.37	13.8	12.8		4670.	[30]
RX-23-AA	1.424	8.64	8.55	21.0	23.0	2900.	2800.	[10][34]
RX-23-AB	1.356	7.48	7.39	17.0	15.8	4000.	2360.	[10][34]
RX-23-AC	1.136	7.88	7.80	18.1	15.1	2180.	2230.	[10][34]
TATB	1.860	>7.75 ^a	8.07	25.9	26.9		2940.	[16]
TNGU	1.885		9.09	37.0	35.7		4250.	[10]
TNM	1.650	6.45	6.67	15.5	15.6	2840.	2450.	[10][34]
TNT	1.632	6.94	6.94	21.6	26.1		3660.	[10][31]
TNT	1.400	6.33	6.28	16.0	13.8	3520.	3690.	[31][32][37]
average difference (calc./expt.- 1)			-0.1% ^b		-3.9%		-6.3%	
standard. deviation			1.4% ^b		8.1%		15.8%	

^a See discussion in the text and Refs. [23] and [24]^b Values computed excluding detonation velocities of PBX9502 and TATB

The average difference between the calculated and experimental detonation pressures is .3.9%, with a standard deviation of 8.1%, **all** within typical experimental **uncertainties**. It **has** been shown that measurements **of the** detonation pressure are less accurate **than** those of the detonation velocity and that **there are significant** variations in the results obtained by different methods [10] [25]. The difficulties **are** due in part to the fact that **the CJ** state, which is preceded by the von Neumann **spike and** immediately followed by the Taylor (release) wave, is not easy to **pinpoint**, even in numerical simulations. **In** fact, many of the “experimental” values given in Table 2 are only estimates based upon cylinder tests [10], which are not particularly sensitive to the detonation pressure [21]. These matters are discussed further in Sec. 3.3, where it is shown that the detonation pressure for **LX14** is probably lower than the value given in Table 2.

Measurements of the detonation temperature are fewer and much less accurate than those of either the velocity or the pressure. **The** data for transparent liquids, especially ones having a small reaction zone, are the most reliable; measurements for solid explosives have additional complications due to being opaque **and** having hot spots [10]. For liquid NM, Refs. [35] and [36] report 13 experiments giving an average of 3470K, with a standard deviation of 190K and a total spread of 780K. Temperature measurements have also been reported for the liquids TNM, RX-23-AA, **RX-23-AB**, and RX-23-AC [34]. The reported measurements for solid PETN [33] [35] [36] [38] show a spread of about 600K and appear to be reasonable and consistent for initial densities in the range $1.6 < \rho_0 < 1.77$. However, there is a larger spread in the **reported** data for the solids TNT and HMX [35] [36] [37][38]. Moreover, the measurements of **Huisheng**, et al. [38], for TNT and HMX at high initial densities, are inconsistent with the data for lower densities and need to be checked. The calculated detonation temperatures are well within the experimental uncertainties for all but one of the explosives shown in Table 2- the experimental value for **RX-23-AB**, which is inconsistent with those for RX-23-AA and RX-23-AC, is likely to be erroneous [3].

3.2 Cylinder Tests

The calculated results for a 1-in cylinder test on PBX9404 [16][22] are shown in Figs. 3 and 4. Figure 3 compares the velocity vs. radius curves obtained using both the PANDA EOS and the JWL EOS with the experimental data. The two calculations are almost indistinguishable from one another and in excellent agreement with the measurements at early times. For radial expansions greater than 1.8 cm, the PANDA EOS predicts slightly higher velocities and gives better agreement with the data than JWL. For completeness, the velocity vs. time and radius vs. time curves for the PANDA calculation are shown in Figs. 4a and 4b, respectively. As expected, the agreement here is also excellent.

Calculations for LX14, another **HMX-based** explosive having a composition **and** properties similar to those of PBX9404, are shown in Fig. 5. Velocity vs. radius **curves** for both a 1-in test [16][21] **and** also a 2-in test [22] are shown in Fig. 5a. (The **wall** thickness was 0.26 cm in both cases.) Once again, the calculated results are in excellent agreement with the experimental data. Figure **5b** compares the calculated velocity vs. time for the 2-in test with high precision measurements obtained using a **Fabry-Perot** interferometer [21]. Results obtained with both standard zoning ($A_x=0.02$ cm, $A_y=0.05$ cm) and finer zoning ($\Delta x=0.01$ cm, $A_y=0.02$ cm) are shown. **The** agreement with experiment is good, although

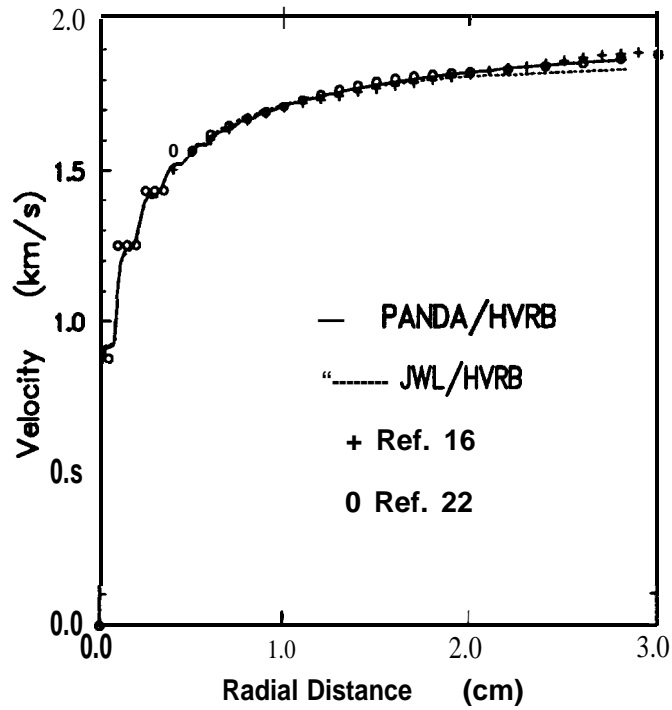


Fig. 3. Velocity vs. radius for PBX9404 cylinder test [16] [22]. Calculations using both PANDA and JWL EOS are shown.

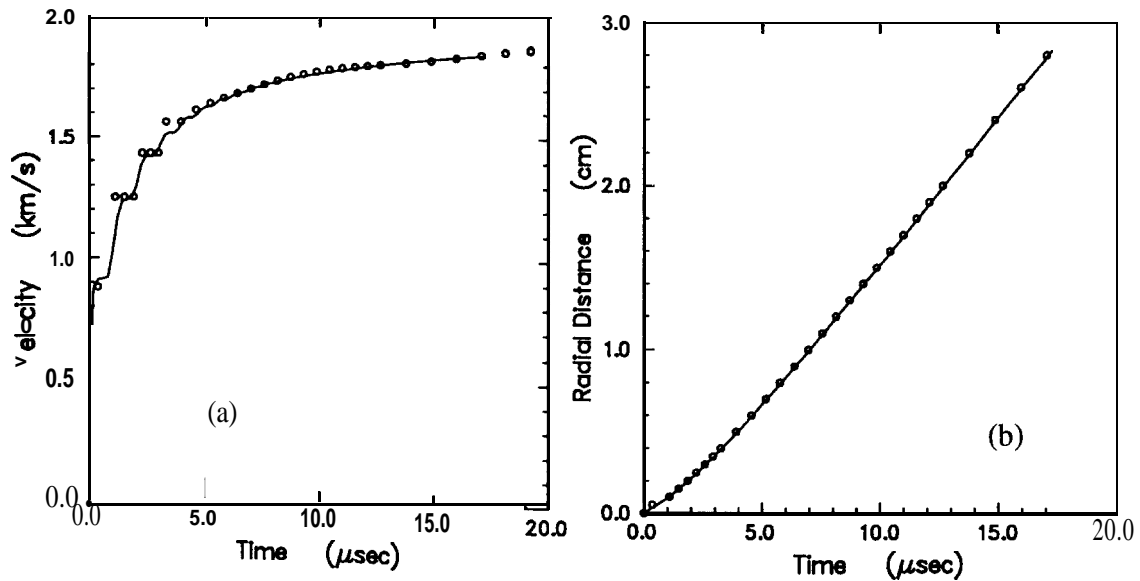


Fig. 4. Velocity vs time (a) and radius vs. time (b) for PBX9404 cylinder test [22]. (PANDA results only)

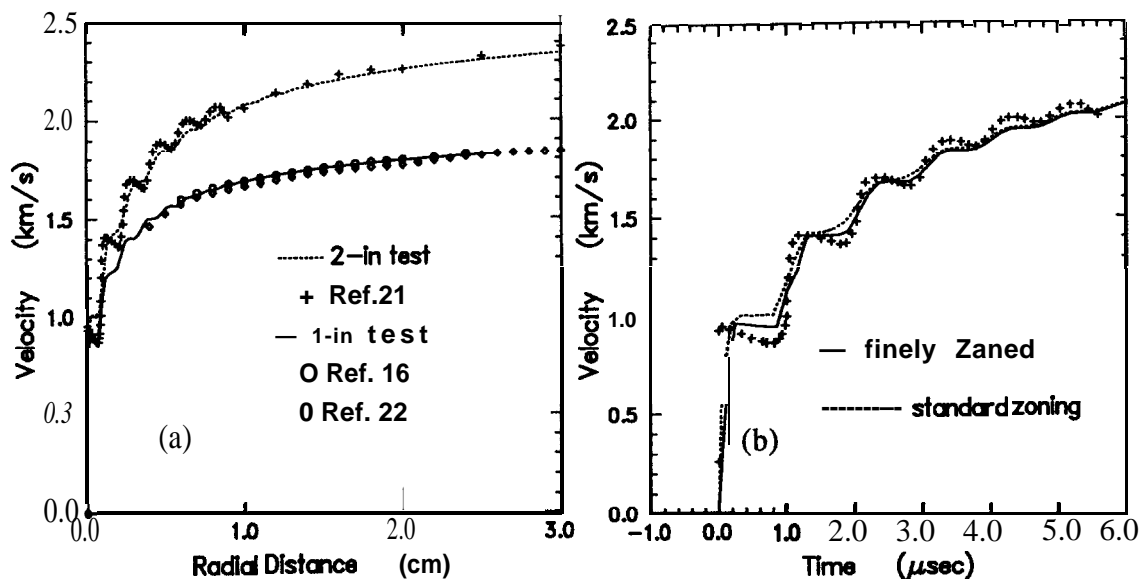


Fig. 5. Cylinder test data for LX-14: (a) - velocity vs. radius for 1-in test [16][22] and 2-in test [21]; (b) - velocity vs. time for 2-in test [21].

even the more finely-zoned calculation does not resolve the velocity oscillations with as much precision as the measurements.

Figure 6 shows the effect of additive content on the cylinder test results for three HMX-based explosives - 100% HMX, PBX-9501 (95% HMX), and PBX9011 (90% HMX). The additives reduce the cylinder wall velocity of HMX by $\sim 6\%$ and $\sim 10\%$ for PBX9501 and PBX9011, respectively. The calculations agree quite well with the experimental data [1][16] in all three cases, showing that the model accurately describes effects due to small changes in chemical composition.

Figure 7 shows the cylinder test results for three RDX-TNT mixtures - pure TNT, Comp B, Grade A (64% RDX, 36% TNT), and Cyclotol (77% RDX, 23% TNT). Since no cylinder test data are available for RDX, the data for HMX are also shown. (The cylinder test results for RDX and HMX should be identical except for a small effect due to different loading densities.) Adding RDX to TNT increases the wall velocity by $\sim 15\%$ and $\sim 20\%$ for Comp B and Cyclotol, respectively. As in Fig. 5, the calculations are in good agreement with the experimental data [1] for all four cases, showing that the model accurately predicts the effects of variations in explosive composition.

Figure 8 shows cylinder test results for HNS at loading densities ranging from 1.0 to 1.68 g/cm^3 . (Note that all of the curves were computed using the *same* EOS table, instead of using a separate EOS fit for each density, as is usually done with the JWLF formula.) The calculated wall velocities are slightly higher than the experimental ones [27] (by $\sim 2\%$ at the highest density and by $\sim 4\%$ at the lowest density). However, the model accurately predicts the drop in cylinder wall velocity with increasing porosity.

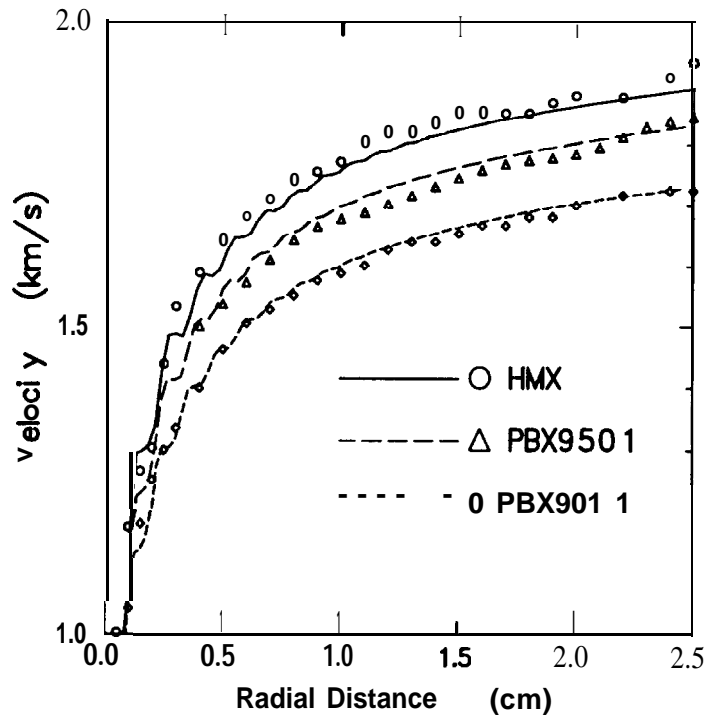


Fig. 6. Cylinder test data for three HMX-based explosives. Experimental data are from Refs. [1] and [16].

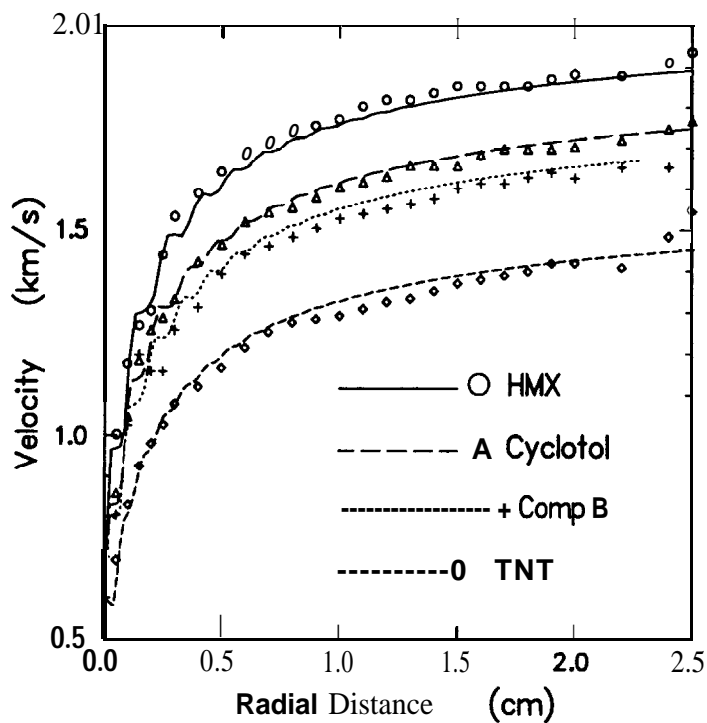


Fig. 7. Cylinder test results for RDX-TNT mixtures. Experimental data are from Ref. [1].

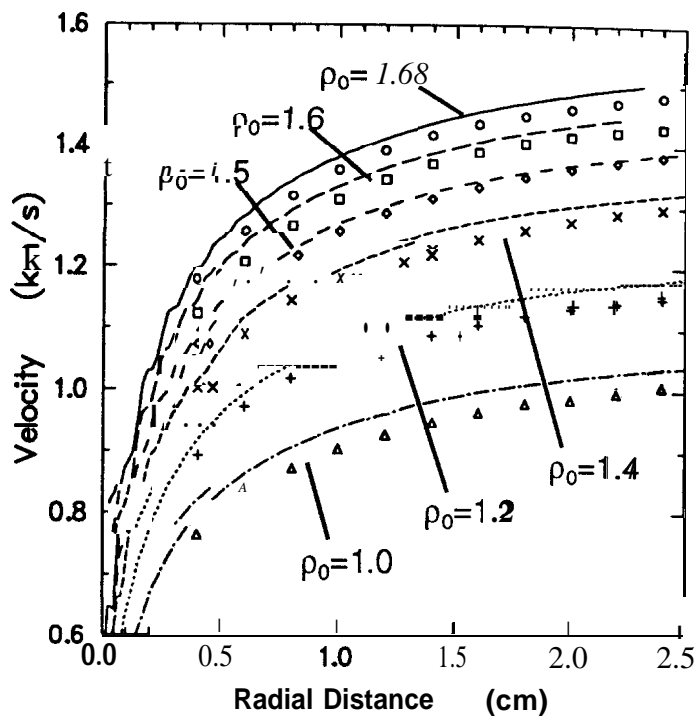


Fig. 8. Cylinder test results for HNS at various loading densities, Experimental data are from Ref. [27].

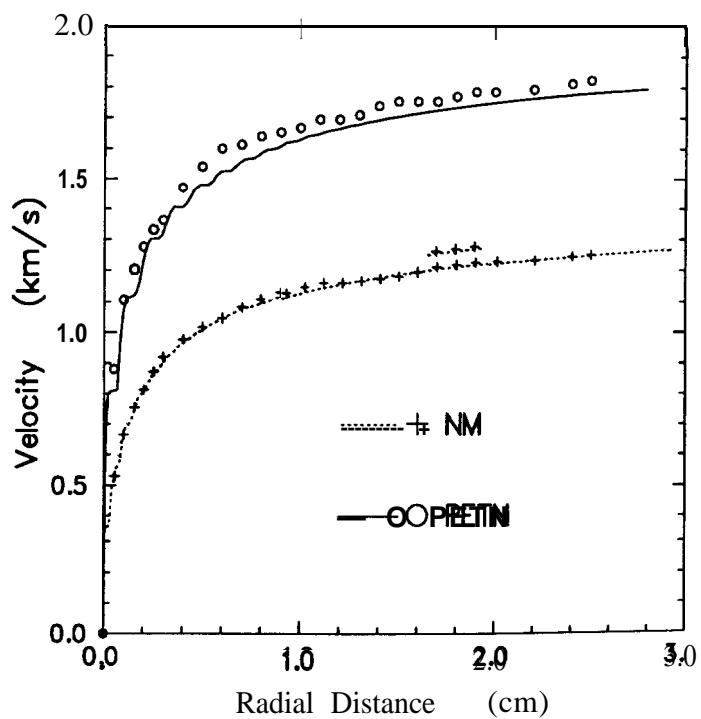


Fig. 9. Cylinder test results for PETN and NM. Experimental data are from Ref. [1].

The cylinder test results for PETN and NM are displayed in Fig. 9. The calculations are also in very good agreement with the measurements [1] for these two cases.

Figure 10 shows the velocity vs. radius curves for both 1-in [16] and 2-in [39] cylinder tests of the TATB-based explosive, PBX-9502. (The wall thickness was 0.26 cm in both cases.) The calculated curves have the correct shape but lie above the experimental ones by -6% and .3% for the 1-in and 2-in tests, respectively. These discrepancies are consistent with the results for the detonation velocity and are larger than those obtained for the other explosives studied.

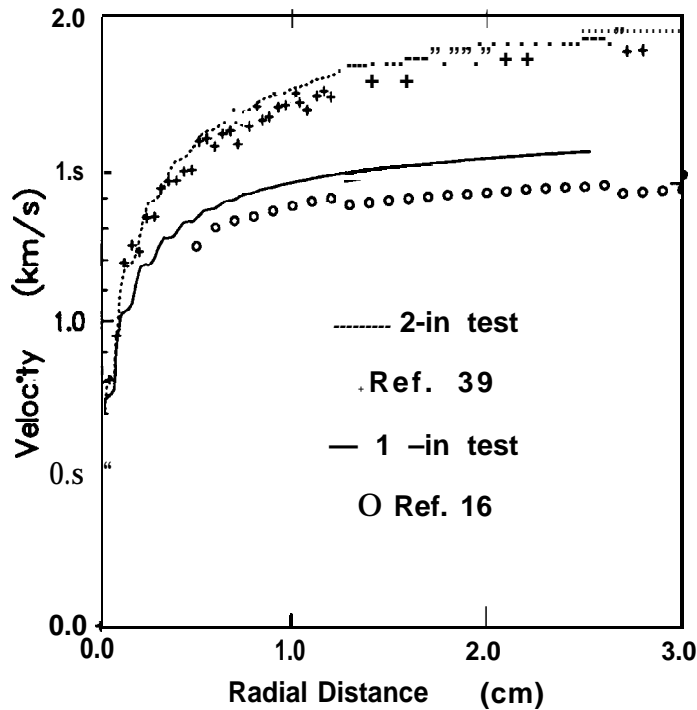


Fig. 10. 1-in and 2-in cylinder test results for PBX9502.

As noted in Sec. 3.1, TATB-based explosives exhibit nonideal behavior in that the infinite diameter detonation velocity is not attained for charge diameters as large as 13 cm [23] [24]. Nonideal behavior has also been seen in interface velocity and plate-push experiments on TATB explosives [40][41] [42]. The velocity (or energy) imparted to the target by the explosive is observed to increase with the length of the charge. Tang [42] has shown that these data can be reproduced using a two-step reactive burn model; about 85% of the energy is released by a fast reaction, which takes 20 ns, while the rest of the energy is released by a slow reaction that requires an additional 240 ns. The total reaction zone length in Tang's model is about 0.2 cm, which is comparable to the wall thickness in the cylinder tests. The slow reaction must also play a role in determining the effect of diameter on the detonation velocity and cylinder wall velocity.

In principle, the effects of nonideal behavior can be treated through the reactive burn model. However, the HVRB model used here was calibrated using shock initiation data and

does not include any slow reaction. Therefore it gives only a rough description of the reaction zone. Preliminary calculations show that adding a slow reaction to the HVRB model does improve the cylinder test predictions. However, a complete study of this problem is beyond the scope of the present work.

A summary of all the cylinder test calculations is given in Table 3. The wall velocities are tabulated at radial displacement of 0.6, 1.25, and 1.9 cm, **corresponding** to volumetric expansions of -2, -4, and -7, respectively. In addition to the explosives shown in Figs. 2 through 10, the table gives results for 11 explosives considered in Ref. [10], for which detailed velocity histories were not available to the present authors. Five of these - **TATB**, **TNGU**, **NE**, **HNO₃#1**, and **HNO₃#2** - are CHNO compositions. Three of them - **BTF**, **HNB**, and **TNM** - are CNO compositions. The other three - **RX-23-AA**, **RX-23-AB**, and **RX-23-AC** - are HNO compositions.

As shown in Table 3, the average difference between the calculated and experimental cylinder wall velocities at 0.6-cm expansion is only **0.2%**, with a standard deviation of **2.8%**. The results are essentially the same for the 1.25- and 1.90-cm expansions, showing that the shapes of the velocity vs. radius curves are predicted correctly. As noted above, the TATB-based explosives show larger deviations than the others, probably because of **non-ideal** behavior. HNB, low density HNS, and RX-23-AA also show deviations of **~4%**, somewhat larger than average.

3.3 Plate Acceleration Tests

Lee, **et al.** [21] studied the motion of metal walls driven by the **HMX-based** explosive LX 14 in flat plate geometries as well as in cylinder tests. They found that the JWL EOS parameters previously derived from cylinder tests did not give satisfactory results when used to calculate the flat plate tests. They concluded that the cylinder test measurements sample the detonation product EOS at densities $\rho < \rho_0$ (where p_0 is the initial explosive density), while the flat plate tests are also sensitive to the EOS at higher compressions, $\rho_0 < \rho < \rho_{CJ}$. They also found that higher plate velocities were obtained for thinner plates, indicating the influence of the reaction zone. By reducing the **CJ** pressure from 37 GPa to 36 GPa, they derived a new set of JWL parameters that fit both the cylinder test data and the plate data for thicknesses greater than 0.05 cm. However, they were not able to fit all of the thin plate data, even using a reactive burn model.

Figure 11 compares the velocity history calculated using the PANDA EOS with two **Fabry-Perot** records for a copper plate of thickness 0.0526 cm, driven by a 1.995-cm thickness of explosive. The predictions agree very well with the measurements, even though the PANDA EOS has a **CJ** pressure of only 33.8 GPa, in contrast to the value of 36 GPa obtained in Ref. [21]. The CTH input file for this problem is given in Appendix C. As discussed below, the results for this test are much less sensitive to the reactive burn model than for the tests using thinner plates. This problem was found to be rather sensitive to zoning; in order to obtain good resolution, a zone size of 0.001 cm was used in the vicinity of the copper plate, while graded zoning was used in the outer parts of the computational mesh.

Cylinder Test Predictions Using Panda EOS

TABLE 3: Summary of copper cylinder wall velocity calculations. All calculations were for 1-in diameter, 0.26-cm wall thickness, except where indicated. $R-R_0$ is the cylinder radius minus the initial radius.

Explosive	Initial Density (g/cm ³)	-----Wall Velocity (ids)-----						Refs.
		$R-R_0=0.6$ cm		$R-R_0=1.25$ cm		$R-R_0=1.9$ cm		
		expt.	calc.	expt.	calc.	expt.	calc.	
BTF	1.852	1.605	1.634	1.755	1.770	1.835	1.839	[10]
Comp B (Gr. A)	1.717	1.439	1.447	1.556	1.588	1.640	1.648	[1]
Cyclotol (77/23)	1.754	1.516	1.519	1.640	1.652	1.695	1.714	[1]
HMX	1.894	1.650	1.649	1.820	1.800	1.883	1.860	[1][10]
HMX	1.188	1.173	1.149	1.314	1.287	1.384	1.348	[10]
HNB ^a	1.965	1.700	1.600	1.880	1.808	1.955	1.885	[10]
HNO ₃ #1	1.542	1.295	1.279		1.452		1.531	[10]
HNO ₃ #2	1.560	1.210	1.245	1.370	1.400		1.470	[10]
HNS	1.681	1.255	1.283	1.385	1.416	1.458	1.476	[27]
HNS	1.402	1.081	1.116	1.207	1.239	1.266	1.294	[27]
HNS	1.001	0.817	0.861	0.931	0.967	0.981	1.013	[27]
LX09	1.840	1.649	1.595	1.758	1.743	1.828	1.804	[22]
LX14 (X-0282)	1.835	1.587	1.584	1.713	1.726	1.777	1.787	[16][22]
LX14 (2-in)	1.835	1.963	1.911	2.152	2.140	2.260	2.249	[21]
NM ^b	1.13	1.045	1.047	1.180	1.165	1.230	1.219	[1][10]
NNE ^b	1.034	0.836	0.859	0.935	0.960	0.990	1.010	[10]
PBX9011	1.770	1.504	1.508	1.633	1.637	1.681	1.697	[1]
PBX9404	1.840	1.603	1.588	1.734	1.737	1.793	1.796	[16][22]
PBX9501	1.834	1.570	1.590	1.707	1.734	1.776	1.795	[16]
PBX9502	1.894	1.301	1.364	1.398	1.475	1.435	1.520	[16]
PBX9502 (2-in)	1.880	1.565	1.624	1.759	1.809	1.827	1.885	[39]
PETN	1.765	1.560	1.524	1.705	1.670	1.790	1.739	[1][10]
PETN	1.498	1.355	1.306	1.510	1.465	1.590	1.538	[10]
PETN	1.266	1.156	1.145	1.304	1.295	1.382	1.364	[10]
RX-23-AA ^b	1.424	1.320	1.299	1.473	1.401	1.520	1.446	[10]
RX-23-AB	1.356	1.080	1.052	1.180	1.145	1.210	1.184	[10]
RX-23-AC	1.136	1.075	1.072	1.170	1.162	1.220	1.195	[10]
TATB ^b	1.83	1.300	1.362	1.403	1.480	1.453	1.530	[10]
TNGU	1.885	1.600	1.558	1.750	1.703	1.825	1.775	[10]
TNM	1.650	1.000	1.019	1.095	1.103	1.130	1.135	[10]
TNT ^b	1.632	1.210	1.231	1.355	1.362	1.410	1.420	[1][10]
average difference (calc./expt.-1)			+0.2%		+0.3%		0.0%	
standard. deviation			2.8%		2.6%		2.6%	

^a Experimental data are for 3/4-in diameter, scaled to 1-in [10].

^b Experimental data are for 2-in diameter, scaled to 1-in [10].

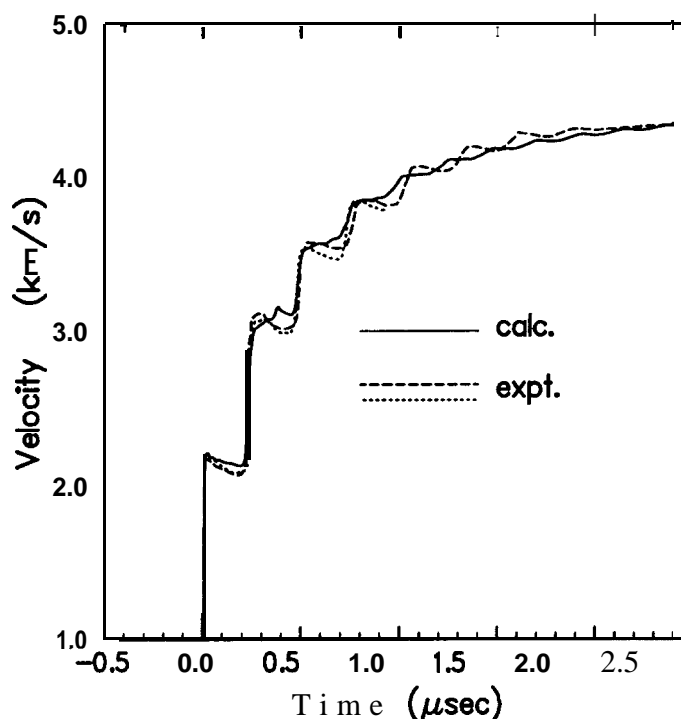


Fig. 11. LX14 flat plate tests #9633 and 9634 of Ref. [21]. HE thickness - 1.995 cm, copper thickness -0.0526 cm, zone size -0.001 cm in vicinity of copper plate.

Analysis of the flat plate experiments illustrates the difficulty of obtaining the CJ pressure from experimental data. The plate motion at early times is determined primarily by the leading part of the detonation wave (including the reaction zone), while the motion at later times depends upon the detonation product expansion and also the thickness of the explosive. Figure 12 shows the initial acceleration of the copper plate (the first plateau in the velocity time history), for the 19 experiments reported in Ref. [21]. It can be seen that the initial velocity is $\sim 2.1 \pm 0.1$ km/s, independent of thickness, for thicknesses greater than 0.01 cm, indicating that the reaction zone has a relatively small effect. However, the higher velocity obtained for a thickness of 0.0025 cm suggests the presence of a von Neumann spike. The ratio R of the copper thickness to the explosive thickness is also indicated. There is no correlation with explosive thickness within the scatter in the data.

The initial plate velocity can be estimated by impedance matching, using the diagram shown in Fig. 13. The Hugoniot for the explosive detonation products is shown by the solid line, with the CJ state denoted as point A. The initial shock state in the copper plate, point B, corresponds to the intersection of the copper Hugoniot with the second shock Hugoniot for the detonation products. The free surface velocity of the copper plate corresponds to zero pressure on the copper release curve, point C. Using the PANDA EOS for the detonation products and the Mie-Grüneisen EOS for copper, the velocity obtained is 2.14 km/s, in good agreement with the experimental data, as shown by the dotted line in Fig. 12. This calculation is only approximate because it ignores the effects of the Taylor wave and the reaction zone. However, it shows that the plate motion is determined not

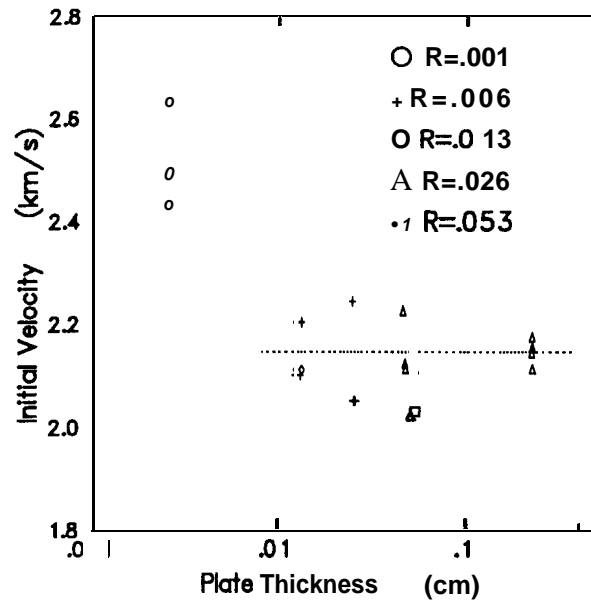


Fig. 12. Initial acceleration of copper plate for experiments reported in Ref. [21]. R is the ratio of the copper plate thickness to the thickness of the explosive. The dotted line shows a velocity of 2.14 km/s, computed as described in the text.

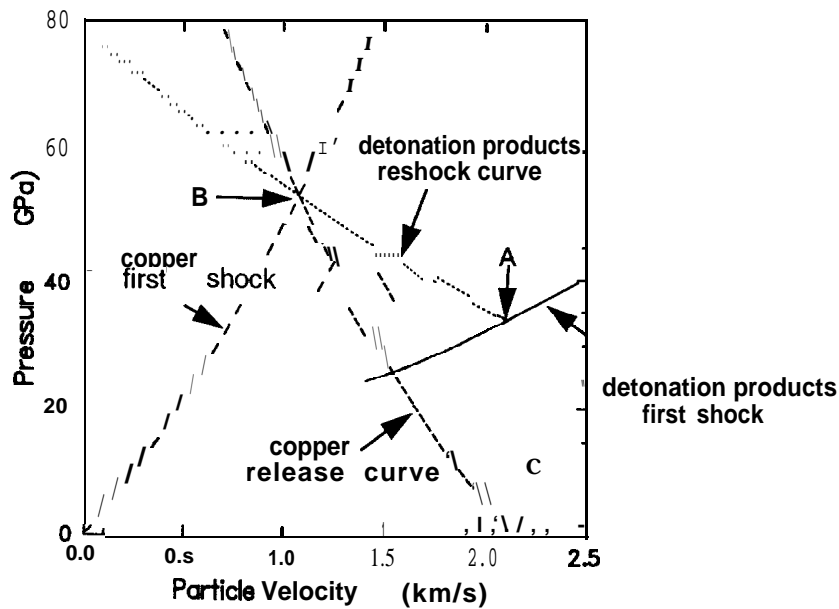


Fig. 13. Impedance matching diagram for interaction of copper plate with LX14 explosive. Point A is the CJ state for explosive, B is shock state in the copper and reshock state in detonation products, C is release state in the copper.

only by the CJ state, but also by the **reshock** behavior of the detonation products. That fact explains why two EOS having quite different **CJ** pressures can give similar results for the plate motion.

A reasonable description of the reaction zone is needed for the experiments involving very thin plates. In the HVRB model, the parameters that have the greatest effect on the reaction zone are the EOS for the **unreacted** explosive (which determines the von Neumann spike pressure) and the constant P_r in Eq. (4) (which determines the overall zone length). However, the HVRB model was developed primarily for modeling shock initiation phenomena, and Eqs. (1)-(4) were not derived to give an accurate description of the reaction zone. The values obtained by calibrating the model to shock initiation data, as described in Sec. 2.3, do not give satisfactory results when extrapolated into the present regime, overestimating the effects of the reaction zone on the plate velocity. Since there are no independent measurements that can be used to determine the necessary parameters, the value of P_r was adjusted to match the initial velocity of a 0.00254 cm copper plate, while the other bum parameters were unchanged from their original values. The adjusted value of P_r (about 1/5 of the original value) was used in the calculation shown in Fig. 11; the velocities obtained using the original value of P_r were -3% higher.

Figure 14 compares the calculated curves with experimental data for a 0.00254 cm copper plate, using the adjusted value of P_r . The theoretical results agree with measurements at both early times, as expected, and also at late times, where the velocity depends on the detonation product expansion and the explosive thickness. The results for an intermediate copper thickness of 0.0126 cm are shown in Fig. 15. The calculated velocities are in satisfactory agreement with experiment, given the scatter in the data (data for the other tests at this thickness show variations of -4% [21]).

The fact that the PANDA model gives good agreement with both flat plate and cylinder tests, which sample different regions of the EOS surface, is further evidence of its **generality**. It may be possible to improve the calculations for thin plates by refining the reactive bum model.

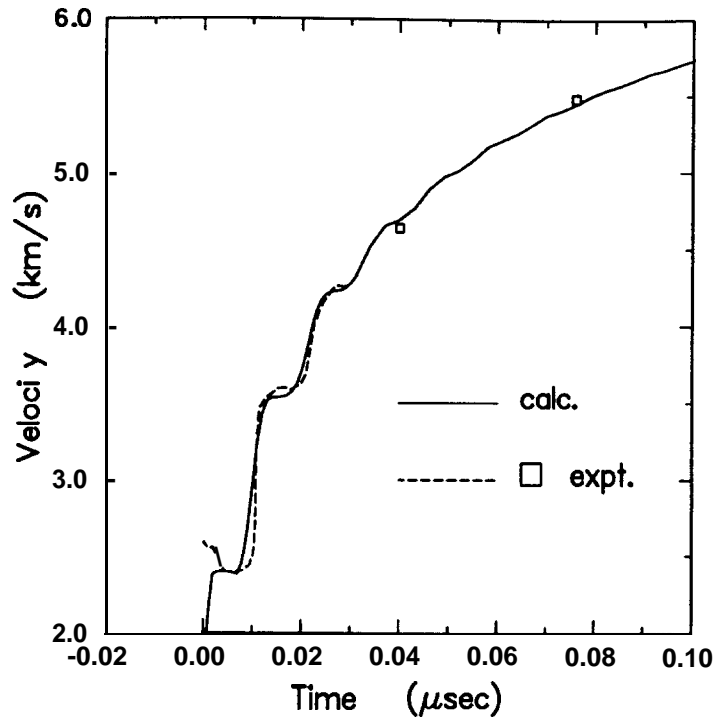


Fig. 14. LX 14 flat plate test #9643 of Ref. [21]. HE thickness - 2.558 cm, copper thickness -0.00254 cm, zone size -0.0002 cm in vicinity of copper plate.

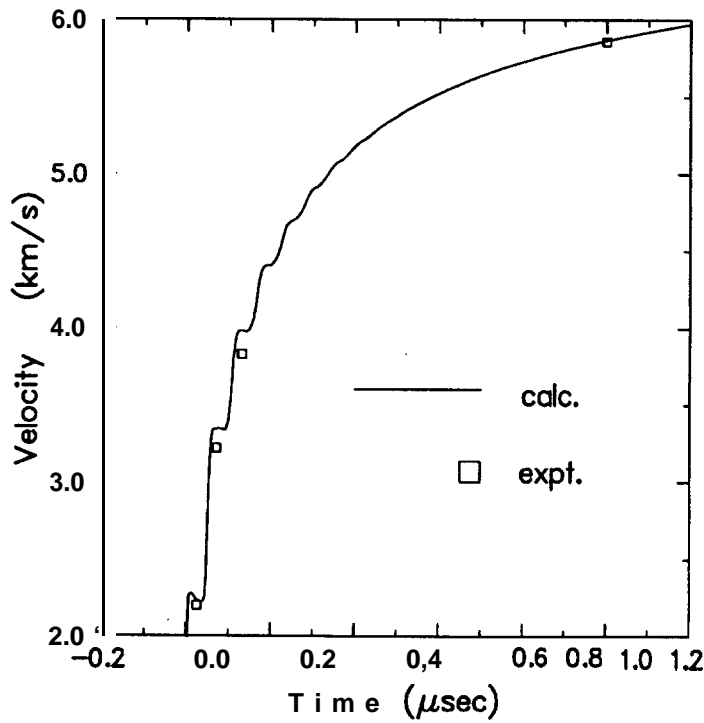


Fig. 15. LX 14 flat plate test #9526 of Ref. [21]. HE thickness - 1.997 cm, copper thickness -0.0126 cm, zone size -0.0005 cm in vicinity of copper plate.

4. Summary and Conclusions

Accurate EOS for explosive detonation products, and the means for using these EOS in hydrocode calculations, are needed in many practical applications which involve the modeling of explosives and other energetic materials. Until recently, analysts have often had to rely on simple analytical EOS formulas for the study of complicated problems. A sophisticated tabular EOS package and reactive burn model [20], which was recently developed for the CTH hydrocode, offers a more realistic treatment of explosives than was previously available. This capability has been used in the present study.

The present work and previous studies [7][8] have demonstrated that the PANDA code can be used to construct accurate *a priori* EOS for the detonation products of CHNO explosives. The PANDA EOS are in very good agreement with experimental detonation properties, overdriven shock data, cylinder test expansion measurements and plate push tests. Hence one advantage of the PANDA code is that it provides a way to predict the EOS for new compositions. By contrast, the analytic JWL formula must be fit to experimental data for each explosive.

It is equally important to recognize that the PANDA code predicts a very different EOS surface from the one obtained with the JWL formula, even though the two models may give comparable results for cylinder tests. Because the PANDA model incorporates the fundamental physics and chemistry of the problem, it is reliable over a wide range of conditions. By contrast, it is well known that JWL parameters obtained from cylinder tests often give poor results in plate push tests, in overdriven shock experiments, and in other problems outside the region of calibration [11][21]. These difficulties arise because of the simplicity of the JWL expression, i.e. the use of a constant specific heat and Grüneisen parameter. The availability of a tabular EOS package eliminates the need to fit the EOS to an analytic function.

Reactive burn phenomena have been relegated to a secondary role in the present study, but certain points should be noted. First, the predicted detonation properties and cylinder wall velocities for TATB-based explosives show larger discrepancies with experiment than do the other explosives. Some of these discrepancies are clearly due to nonideal behavior, which has been observed in the effect of diameter on detonation velocity [23] [24] and the effect of charge length on the energy imparted to a target [40] -[42]. Second, the velocity histories of thin plates accelerated by LX 14 also show effects due to the reaction zone [21]. These problems show that the detonation product EOS can be separated from reactive burn phenomena only to a first approximation. However, a full analysis of reactive effects would have required more time than could be devoted to the present study.

References

- [1] E. L. Lee, H. C. Homig, and J. W. Kury, "Adiabatic Expansion of High Explosive Detonation Products," report UCRL-50422, Lawrence Radiation Laboratory, Livermore, CA, May 2, 1968.
- [2] C. L. Mader, Numerical Modeling of Detonations (University of California, Berkeley, 1979).
- [3] M. Finger, E. Lee, F. H. Helm, B. Hayes, H. Homig, R. McGuire, and M. Kahara, "The Effect of Elemental Composition on the Detonation Behavior of Explosives," in Proceedings of the Sixth Symposium (International) on Detonation, edited by D. J. Edwards, ACR-221 (Office of Naval Research, Department of the Navy, 1976), pp. 710-722.
- [4] M. Cowperthwaite and W. H. Zwisler, "The JCZ Equations of State for Detonation Products and Their Incorporation into the TIGER Code," in Proceedings of the Sixth Symposium (International) on Detonation, edited by D. J. Edwards, ACR-221 (Office of Naval Research, Department of the Navy, 1976), pp. 162-170.
- [5] R. Chirat and G. Pittion-Rossillon, "A New Equation of State for Detonation Products," J. Chem. Phys. 74, 4634-4642 (1981).
- [6] F. H. Ree, "Postdetonation Behavior of Condensed High Explosives by Modern Methods of Statistical Mechanics," in Proceedings of the Seventh Symposium (International) on Detonation, edited by J. M. Short, NSWL MP 82-334 (Naval Surface Weapons Center, White Oak, MD, 1981), pp. 646-660.
- [7] G. I. Kerley, "Theoretical Equations of State for the Detonation Properties of Explosives," in Proceedings of the Eighth Symposium (International) on Detonation, edited by J. M. Short, NSWL MP 86-194 (Naval Surface Weapons Center, White Oak, MD, 1986), pp. 540-547.
- [8] G. I. Kerley, "Theoretical Model of Explosive Detonation Products: Tests and Sensitivity Studies," in Proceedings of the Ninth Symposium (International) on Detonation, edited by W. J. Morat, OCNR 113291-7 (Office of the Chief of Naval Research, 1990), pp. 443-451.
- [9] M. L. Hobbs and M. R. Baer, "Nonideal Thermodynamic Calculations Using a Large Product Species Data Base," Sandia National Laboratories report SAND-2-0482, 1992.
- [10] P. C. Souers and J. W. Kury, "Comparison of Cylinder Data and Code Calculations for Homogeneous Explosives," report UCRL-JC-110661, Lawrence Livermore National Laboratory, Livermore, CA, May 1992.

- [11] E. L. Lee, M. Van **Thiel**, L. G. Green, and A. Mitchell, "Detonation Product EOS: The Region Above **Chapman-Jouget** Pressure," Proceedings of the APS 1983 Topical Conference on Shock Waves in Condensed Matter, edited by J. R. Asay, R. A. Graham, and G. K. **Straub** (North-Holland, New York, 1984) p. 617.
- [12] G. I. **Kerley**, "User's Manual for **PANDA II**: A Computer Code for Calculating Equations of State," **Sandia** National Laboratories report **SAND88-2291**, 1991.
- [13] G. I. **Kerley**, "A Model for the Calculation of Thermodynamic Properties of a Fluid Using Hard-Sphere Perturbation Theory and the Zero-Kelvin Isotherm of the Solid," in Molecular Based Study of Fluids, edited by J. M. **Haile** and G. A. **Mansoori** (Am. Chem. Soc., Washington, DC., 1983) pp 107-138.
- [14] G. I. **Kerley**, "Equations of State and Gas-Gas Phase Separation in Soft Sphere **Mixtures**," *J. Chem. Phys.* 91, 1204-1210 (1989).
- [15] B. M. **Dobratz** and P. C. Crawford, "LLNL Explosives **Handbook**," Lawrence Livermore National Laboratory report UCRL-52997, January 1985.
- [16] T. R. Gibbs and A. **Populato**, LASL Explosive Property Data (University of California, Berkeley, 1980).
- [17] J. M. **McGlaun**, F. J. Ziegler, S. L. Thompson, L. N. Kmetyk, and M. G. **Elrick**, "CTH - User's Manual and Input Instructions," **Sandia** National Laboratories report **SAND88-0523**, April 1988.
- [18] E. S. **Hertel, Jr.**, "A Comparison of the CTH Hydrodynamics Code With Experimental Data," Sandia National Laboratories report **SAND92-1879**, September 1992.
- [19] G. I. **Kerley**, "CTH Reference Manual: The Equation of State Package," **Sandia** National Laboratories report **SAND91-0344**, 1991.
- [20] G. I. **Kerley**, "CTH Equation of State Package: Porosity and Reactive Burn Models," Sandia National Laboratories report **SAND92-0553**, 1992.
- [21] E. Lee, D. **Breithaupt**, C. **McMillan**, N. Parker, J. **Kury**, C. Tarver, W. Quirk, and J. Walton, "The Motion of Thin Metal Walls and The Equation of State of Detonation Products," in Proceedings of the Eighth Symposium (International) on Detonation, edited by J. M. Short, NSWL MP 86-194 (Naval Surface Weapons Center, White Oak, MD, 1986), pp. 613-624.
- [22] E. L. Lee, F. H. Helm, M. Finger, and J. R. Walton, "Equations of State for Detonation Products of High Energy PBX Explosives," report **UCID-17540**, Lawrence Livermore Laboratory, Livermore, CA, Aug. 1, 1977.
- [23] A. W. Campbell, "Diameter Effect and Failure Diameter of a TATB-Based Explosive," *Propellants, Explosives, Pyrotechnics* 9, 183-187 (1984).

- [24] C. D. Hutchinson, G. C. W. Foan, H. R. Lawn, and A. G. Jones, "Initiation and Detonation Properties of the Insensitive High Explosive TATB/Kel-F 800 95/5," in Proceedings of the Ninth Symposium (International) on Detonation, edited by W. J. Morat, OCNR 113291-7 (Office of the Chief of Naval Research, 1990), pp. 123-132.
- [25] K. K. Shvedov, "Determination of the Chapman-Jouguet Parameters in the Detonation of Condensed Explosives," Combustion, Explosives, and Shock Waves 23,464-474 (1987).
- [26] D. J. Steinberg, "Comparison of Experimental Data on Detonation Velocity and Chapman-Jouguet Pressure vs. Initial HE Density With Predictions From Ree's Model Equation of State," in Proceedings of the Eighth Symposium (International) on Detonation, edited by J. M. Short, NS WL MP 86-194 (Naval Surface Weapons Center, White Oak, MD, 1986), pp. 513-520.
- [27] P. E. Kramer, "HNS Cylinder Tests," Mason and Hanger-Silas Mason report MH-SMP-75-17, 1975.
- [28] A. W. Campbell and R. Engelke, "The Diameter Effect in High-Density Heterogeneous Explosives," in Proceedings of the Sixth Symposium (International) on Detonation, edited by D. J. Edwards, ACR-221 (Office of Naval Research, Department of the Navy, 1976), pp 642-652.
- [29] W. C. Davis and J. B. Ramsay, "Detonation Pressures of PBX-9404, Composition B, PBX-9502, and Nitromethane," in Proceedings of the Seventh Symposium (International) on Detonation, edited by J. M. Short, NSWL MP 82-334 (Naval Surface Weapons Center, White Oak, MD, 198 1), pp. 531-539.
- [30] H. C. Hornig, E. L. Lee, M. Finger, and J. E. Kurrle, "Equation of State of Detonation Products," in Proceedings of the Fifth Symposium (International) on Detonation, edited by D. J. Edwards, ACR- 184 (Office of Naval Research, Department of the Navy, 1970), pp. 503-5 11; the detonation pressure for the highest density includes a 6% correction by L. Green, personal communication, 1984.
- [31] M. J. Urizar, E. James, Jr., and L. C. Smith, "Detonation Velocity of Pressed TNT," Phys. Fluids 4,262-274 (1961).
- [32] M. J. Kamlet and C. Dickenson, "Chemistry of Detonations. III. Evaluation of the Simplified Computational Method for Chapman-Jouget Detonation Pressures on the Basis of Available Experimental Information," J. Chem. Phys. 48, 43-50 (1968).
- [33] I. M. Voskoboinikov, and A. Ya. Apin, "Measurement of Detonation Front Temperatures of Explosives," Dokl. Akad. Nauk SSSR 130,805 (1960).
- [34] P. A. Urtiew, "Brightness Temperature of Detonation Wave in Liquid Explosives," Acts Astronautic 3,555-566 (1976).

- [35] Y. Kate, N. Mori, H. Sakai, K. Tanaka, T. Sakurai, and T. Hikita, "Detonation Temperature of Nitromethane and Some Solid High Explosives," in Proceedings of the Eighth Symposium (International) on Detonation, edited by J. M. Short, NSWL MP 86-194 (Naval Surface Weapons Center, White Oak, MD, 1986), pp. 558-566. Also see references cited for nitromethane.
- [36] He Xianchu, Han Chengbung, and Kang Shufong, "The Measurement of Detonation Temperature of Condensed Explosives With Two Colour-Optical Fiber Pyrometer," in Proceedings of the Eighth Symposium (International) on Detonation, edited by J. M. Short, NSWL MP 86-194 (Naval Surface Weapons Center, White Oak, MD, 1986), pp. 567-574. Also see references cited for nitromethane, TNT, and PETN.
- [37] Y. Kate, N. Mori, H. Sakai, T. Sakurai, and T. Hikita, "Detonation Temperature of Some Liquid and Solid Explosives," in Proceedings of the Ninth Symposium (International) on Detonation, edited by W. J. Morat, OCNR 113291-7 (Office of the Chief of Naval Research, 1990), pp. 939-946.
- [38] S. Huisheng, H. Chengbang, K. Shufang, and H. Lihong, "The Studying of Detonation Temperature of Solid High Explosives," in Proceedings of the Ninth Symposium (International) on Detonation, edited by W. J. Morat, OCNR 113291-7 (Office of the Chief of Naval Research, 1990), pp. 947-952.
- [39] E. Baker, personal communication, 1992.
- [40] W. L. Seitz, H. L. Stacy, and J. Wackerle, "Detonation Reaction Zone Studies on TATB Explosives," in Proceedings of the Eighth Symposium (International) on Detonation, edited by J. M. Short, NSWL MP 86-194 (Naval Surface Weapons Center, White Oak, MD, 1986), pp. 123-132.
- [41] W. L. Seitz, H. L. Stacy, R. Engelke, P. K. Tang, and J. Wackerle, "Detonation Reaction-Zone Structure of PBX 9502," in Proceedings of the Ninth Symposium (International) on Detonation, edited by W. J. Morat, OCNR 113291-7 (Office of the Chief of Naval Research, 1990), pp. 657-669.
- [42] P. K. Tang, "Modeling Hydrodynamic Behaviors in Detonation," Propellants, Explosives, Pyrotechnics 16,240-244 (1991).
- [43] S. A. Silling, "CTH Reference Manual: Viscoplastic Models," Sandia National Laboratories report SAND9 1-02923, 1991.
- [44] P. A. Taylor, "CTH Reference Manual: The Steinberg-Guinan-Lund Viscoplastic Model," Sandia National Laboratories report SAND92-07 16, 1992.

Appendix A

PANDA Input File for PBX9404

```

|*****
!
! 06/18/93 - EOS for detonation products of PBX-9404.
! PBX-9404 is 94% HMX, 3% NC, 3% CEF by weight.
! Formula - c[1.40]h[2.75]n[2.57]o[2.69]cl[.03]p[.01] (100 g of
! explosive) - the cl and p are ignored in this setup.
! heat of formation (298K) = 0.00331 (Dobratz and Crawford)
!
! Energy zero of EOS tables is assumed to give zero enthalpy for
! elements in their standard states at 1 atm and 298K. Energy zero
! for table is unreacted explosive at 298K.
!
|*****
!
! htf is (-) heat of formation,
! mc, mh2, mn2, and mo2 are moles of c, h2, n2, and O2.
!
s y m htf=-.00331 mc=1.40 mh2=1.375 mn2=1.285 mo2=1.345
!
mod mix ezro=htf
c[1]o[2] ! carbon dioxide
  matid=201 name=co2 file=hesps eshift=-9.1552
n[2] ! molecular nitrogen
  matid=202 name=n2 file=hesps eshift=-.30900 moles=mn2
h[2]o[1] ! water
  matid=203 name=h2o file=hesps eshift=-13.971
c[1]o[1] ! carbon monoxide
  matid=204 name=co file=hesps eshift=-4.2551
c[1]h[4] ! methane
  matid=205 name=ch4 file=hesps eshift=-5.2897
n[1]h[3] ! ammonia
  matid=206 name=nh3 file=hesps eshift=-3.2789
h[2] ! molecular hydrogen
  matid=207 name=h2 file=hesps eshift=-4.1866 moles=mh2
o[2] ! molecular oxygen
  matid=208 name=o2 file=hesps eshift=-.27085 moles=mo2
n[1]o[1] ! nitric oxide
  matid=209 name=no file=hesps "eshift=2.7206
h[2]c[1]o[2] ! formic acid
  matid=301 name=hcooh file=hesps eshift=-8.4598
c[1] ! graphite
  matid=213 name=grp ptyp=.01 file=hesps eshift=59.157 moles=mc
c[1] ! fluid carbon
  matid=210 name=clq ptyp=.01 file=hesps eshift=59.157
c[1] ! diamond
  matid=214 name=dia ptyp=.01 file=hesps eshift=60.057

```

```

n[1]          ! atomic nitrogen
  matid=102 name=n1  file=hesps  eshift=33.294
0[1]          ! atomic oxygen
  matid=108 name=o1  file=hesps  eshift=15. 172
h[1]          ! atomic hydrogen
  matid=107 name=h1  file=hesps  eshift=210.19

!
! Compute CJ state
!
cj mix
1.84

!
! Make EOS table - use set bas command to find FZ and FW

set bas
c[1.40]h[2.75]n[2.57]o[2.69]      ! c1[.03]p[ .011 - ignored

isot mix 3.1635 3.1647 20 1 298 0 1 1
slib mix
201
51.320 99.996 67.280 298 3.16
301
0 0 1 1
.01 .15 2
.1 5 45 2

298 1000 2 1
1.e3 1.e4 24 2

Y
298 .29

8211 061893 b8211 a8211
!
! Read table back in and compute CJ properties

mod sol tab=1
8211 b8211
cj sol
1.84 0 0

end

```

Appendix B

CTH Input File for PBX9404 Cylinder Test

```

*****
*
*           CTH Calculation of PBX9404 Cylinder Test
*           07/28/93
*
* 1 in diameter stick of explosive enclosed in 0.26 cm thick Cu tube.
* 15 cm length of explosive, cylinder expansion studied near 8 cm.
* - X-Mesh: uniform 0.02 cm zones out to 4.0 cm (13 zones in Cu),
*   then graded region out to 6.0 cm.
* - Y-Mesh: uniform 0.05 cm zones from 5.0 to 10.0 cm, graded zones
*   at beginning and end of stick.
* - Histories for recording cylinder expansion at 7, 8, and 9 cm, at
*   surface of Cu wall. Histories for recording of arrival times at
*   7, 8, and 9 cm, along cylinder axis.
* - Uses tabular EOS for detonation products of explosive.
* - Uses HVRB model to propagate detonation wave. Explosive is
*   initiated by a 1.3 cm booster.
*
*****
*eor* genin - CTHGEN input
* Title record
PBX9404 Cylinder Test - Panda EOS, HVRB burn
* Control block
CONTROL
MMP
ENDCONTROL
* Set up geometry and mesh
MESH
BLOCK 1 GEOM=2DC TYPE=E
  Xo 0.0
    x1 W=4 .0 DXF=0.02 DXL=0.02
    x2 W=2.0 DXF=0.02 DXL=0.07
  ENDX
  Yo -1.3
    Y1 W=1.3 DYF=0.25 DYL=0.20
    Y2 W=5.0 DYF=0.20 DYL=0.05
    Y3 W=5.0 DYF=0.05 DYL=0.05
    Y4 W=5.0 DYF=0.05 DYL=0.20
  ENDY
  XACT 0.0 1.5
  YACT -1.3 0.0
ENDB
ENDMESH
* Material insertion inputs
INSERTION of MATERIAL
BLOCK 1

```

```

PACKAGE BOOSTER
  MATERIAL 3
  INSERT BOX
    x1 0.0      x2 1.27
    Y1 -15.0    Y2 0.0
  ENDINSERT
ENDPACKAGE
PACKAGE HE
  MATERIAL 2
  INSERT BOX
    x1 0.0      x2 1.27
    Y1 -15.0    Y2 25.0
  ENDINSERT
ENDPACKAGE
PACKAGE COPPER CASE
  MATERIAL 1
  INSERT BOX
    X1 1.27     x2 1.53
    Y1 -15.0    Y2 25.0
  ENDINSERT
ENDPACKAGE
ENDBLOCK
ENDINSERTION
* EOS input set - new interface
EOS
* Copper - Mie-Gruneisen
MAT1 MGRUN
  R0=8.94 CS=3.94E5 S=1.489 G0=1.99 CV=4.56E10
* PBX9404 Explosive - Panda EOS with HVRB model
MAT2 SESAME EOS=8211 FEOS='sesame'
  RP=1.84 R0=1.873 CS=2.9E5 S=2.0 G0=1.0 CV=1.35E11
  TYP=2.0 PR=5.9E10 ZR=2.36 MR=1.5 PI=0.5E10
  RMAX=5.0 RMIN=0.1 TMAX=5.0 PT=1.0E13
* PBX9404 Explosive - JWJ
MAT3 JWJ
  R0=1.84 AG=8.524 BG=0.1802 CG=0.01207
  R1=4.60 R2=1.30 WG=0.38 PCJ=0.370 DCJ=0.880
ENDEOS
* HEBURN input set
HEBURN
  MAT 3 D=8.80E5
  DL 0.0, -1.3 TO 1.5, -1.3 R=100.0 TIME=0.0
ENDHE
* Elastic-plastic Input set
E PDATA
  MATEP 1 YIELD=3.5E9 POISSON=0.35
  MIX 3
ENDE
*****
*eor* cthin - CTH input
* Title record
PBX9404 Cylinder Test - Panda EOS, HVRB burn
* Control block
CONTROL

```

Cylinder Test Predictions Using Panda EOS

```
TSTOP = 29. 0E-6
RDUMPF = 3600.
CPSHIFT = 999.
NTBAD 100000
ENDC
* Choose fluxing and interface options
CONVCT
CON=1
INT=HIGH
NOFRAGMENT 1
NOFRAGMENT 2
ENDC
* First 3 tracers are near to OD of copper tube
* Second 3 tracers are near to cylinder axis
TRACER
  ADD 1.48,7.0 to 1.48,9.0  N=3  FIXED=Y
  ADD 0.08,7.0 to 0.08,9.0 N=3
ENDT
* Edit specifications
EDIT
SHORTT
  TIME=0.0 DT=5.0E-4
ENDS
LONGT
  TIME=0.0  DT=5.0E-4
ENDL
PLOTT
  TIME=0.0  DT=5.0E-6
ENDP
HISTT
  TIME=0.0  DT=5.0E-8
  HTRACER1
  HTRACER2
  HTRACER3
  HTRACER4
  HTRACER5
  HTRACER6
ENDH
ENDE
* Define boundary conditions
BOUNDARY
BHY
  BL 1
  BXB = 0 , BXT = 1
  BYB = 1 , BYT = 1
ENDB
ENDH
ENDB
* Set minimum and maximum time steps
MINDT
  TIME = 0.  DT = 1.E-11
ENDN
MAXDT
  TIME = 0.  DT = .01
```

```
ENDX
* Fracture input set
FRACTS
  PRESSURE
  PFRAC1 -0.3E10
  PFRAC2 -5.0E6
  PFRAC3 -5.0E6
  PFMIX -0.3E10
  PFVOID -0.3E10
ENDF
```

Appendix C

CTH Input File for LX14 Plate Acceleration Test

```

*****
*
*           CTH Calculation of LX-14 Plate Experiment #9634
*                   08/30/93
* Test data. reported by Lee, et. al., 8th Det. Sym., pp 613-624-
* 1.995 cm thickness of LX-14 accelerates 0.0526 cm Cu plate.
* Explosive initiated by using JWL/programmed burn in first 0.2 cm-
* - Mesh: Zones graded from 0.03 cm down to 0.001 cm for first 1.90
*         cm, then 0.001 cm zones (53 zones in Cu) for 0.6 cm,
*         then graded zones on outer part of mesh.
* - Panda EOS with HVRB for explosive.
*
***** ***** ***** ***** *****
*eor* genin - CTHGEN input
* Title record
PL9634 - /2.0 LX-14/->/0.053 Cu/ Panda/HVRB
* Control block
CONTROL
MMP
* CHECKMESH
ENDCONTROL
* Set up geometry and mesh
MESH
BLOCK 1 GEOM=1DR      TYPE=E
  Xo   0.0
    x1  W=1.90   DXF=0.030  DXL=0.001
    x2  W=0.60   DXF=0.001  DXL=0.001
    x3  W=0.50   DXF=0.001  DXL=0.010
  ENDX
  XACT  -2.0 0.20
ENDB
ENDMESH
* Material insertion inputs
INSERTION of MATERIAL
BLOCK 1
  PACKAGE BOOSTER
  MATERIAL 3
  INSERT BOX
    x1  0.0  x2  0.2
  ENDINSERT
ENDPACKAGE
PACKAGE HE
  MATERIAL 2
  INSERT BOX
    x1  0.2  x2  1.9954
  ENDINSERT

```

```

ENDPACKAGE
PACKAGE COPPER PLATE
  MATERIAL 1
  INSERT BOX
    x1 1.9954 x2 2.048
  ENDINSERT
ENDPACKAGE
ENDBLOCK
ENDINSERTION
* EOS input set - new interface
EOS
* Copper - Mie-Gruneisen
MAT1 MGRUN
  RO=8.94 CS=3.94E5 s=1.489 G0=1.99 CV=4.56E10
* LX14 Explosive - Panda EOS with HVRB model
MAT2 SESAME EOS=8231 FEOS='sesame'
  RP=1.835 R0=1.850 CS=2.9E5 S=2.0 G0=1.0 CV=1.35E11
  TYP=2.0 PR=1.7E10 ZR=2.36 MR=1.5 PI=0.5E10
  RMAX=5.0 RMIN=0.01 TMAX=5.0 PT=1.0E13
* LX-14 Explosive - JWJ
MAT3 JWJ
  R0=1.835 AG=8.261 BG=0.1724 CG=0.01296
  R1=4.55 R2=1.32 WG=0.38 PCJ=0.370 DCJ=0.880
ENDEOS
* HEBURN input set
HEBURN
  MAT 3 D=8.80E5
  DP 0.0 R=100.0 TIME=0.0
ENDHE
* Elastic-plastic Input set
EPDATA
  MATEP 1 YIELD=3.5E9 POISSON=0.35
  MIX 3
ENDE
*****
*eor* cthin - CTH input
* Title record
PL9634 - /2.0 LX-14/->/0.053 Cu/ Panda/HVRB
* Restart instructions
* RESTART
* TIME=2.0E-6
* ENDR
* Control block
CONTROL
  TSTOP = 5.0E-6
  RDUMPF = 3600.
  CPSHIFT = 999.
  NTBAD 100000
ENDC
* Choose fluxing and interface options
CONVCT
  CON= 1
ENDC
* Edit specifications

```

Cylinder Test Predictions Using Panda EOS

```
TRACER
  ADD 2.0455 to 2.0475 N=3
ENDT
EDIT
  SHORTT
    TIME=0.0 DT=5.0e-4
  ENDS
  LONGT
    TIME=0.0 DT=5.0e-4
  ENDL
  PLOTT
    TIME=0.0 DT=0.5e-6
  ENDP
  HISTT
    TIME=0.0 DT=5.E-8
    TIME=2.0E-6 DT=5.E-10
    HTRACER1
    HTRACER2
    HTRACER3
  ENDH
ENDE
* Define boundary conditions
BOUNDARY
  BHY
    BL 1
    BXB = 1 , BXT = 1
  ENDB
  ENDH
ENDB
* Set minimum and maximum time steps
MINDT
  TIME = 0. DT = 1.E-11
ENDN
MAXDT
  TIME = 0. DT = .01
ENDX
* Fracture input set
FRACTS
  PRESSURE
  PFRAC1 -0.3E10
  PFRAC2 -0.3E10
  PFMIX -0.3E10
  PFVOID -0.3E10
ENDF
```

External Distribution

Stanley Klein, M2/321
The Aerospace Corp.
PO Box 92957
Los Angeles, CA 90009-2957

Eric Wong, M4/901
The Aerospace Corp.
PO Box 92957
Los Angeles, CA 90009-2957

R. Blandford
AFTAC/TT/CSS
Suite 1450
1300 N. 17th St.
Arlington, VA 22209

G. R. Johnson
Alliant Techsystems Inc.
7225 Northland Dr.
Brooklyn Park, MN 55428

Eric Peterson
MN1 1-2720
Alliant Techsystems, Inc.
600 Second St., NE
Hopkins, MN 55343

M. Alme
Alme and Associates
102 Stevens Forest Professional Center
9650 Santiago Road
Columbia, MD 21045

J. Walker
Amparo Corporation
P. O. Box 2687
Santa Fe, NM 87504

Frank Maestas
Principal Engineer
Applied Research Associates
4300 San Mateo Blvd.
Suite A220
Albuquerque, NM 87110

Richard Zemow
Applied Research Associates
714 West Jefferson Ave.
Suite 305
Lakewood, CO 80235

Howard Chung
Argonne National Laboratory
RE/331
9700 South Cass Avenue
Argonne, IL 604394817

Ernest L. Baker
Bldg 3022, SMCAR-AEE-WW
u. s. Army **ARDEC**
Picatiny Arsenal, NJ 07806-5000

U.S. Army Research Laboratory (5)
Aberdeen Proving Ground, MD 21005-5066
Attn: R. B. Frey
Attn: K. Kimsey, AMSRL-WT-TC
Attn: R. Lieb, SLCBR-IB-P
Attn: J. Starkenberg
Attn: J. Zukas, AMSRL-WT-TC

John Tipton
U. S. Army Engineer Division
HNDED-SY
PO Box 1600
Huntsville, AL 35807

R. Rohani
U.S. Army Engineer Waterways Experiment
Station
Attn: CEWES-SD
3909 Halls Ferry Road
Vicksburg, MS 39180-6199

Shun-chin Chou
Army Materials Technology Laboratory
SLCMT-MRD
Watertown, MA 02172-0001

George Snyder (2)
U. S. Army Missile Command
AMSMI-RD-ST-WF
Redstone, Arsenal, AL 35898-5247
Attn: J. Billingsley, G. Snyder

Cylinder Test Predictions Using Panda EOS

David Tenenbaum

U. S. Army Tank Automotive Command
RD&E Center
Survivability Division
Mail Code MASTA-RSS
Warren, MI 48397-5000

R. D. Everhart

Battelle Memorial Institute
505 King Ave.
Columbus, OH 43201-2693

Glen Salo

BDM Corporation
1801 Randolph Road SE
Albuquerque, NM 87106

Richard Beyer

Bettis Atomic Power Laboratory
Westinghouse Electric Company
Box 79
West Mifflin, PA 15122-0079

Steven Bishop

Belvoir RD&E Center
STRBE-NAA
Fort Belvoir, VA 22060-560

Kevin Heusen (2), MS 87-60

The Boeing Company
PO Box 3999
Seattle, WA 98124
Attn: K. Heusen, R. Schmidt

T. J. Ahrens

Seismological Laboratory
Division of Geological and Planetary Sciences
California Institute of Technology
Pasadena, CA 91125

S. Schuster

California Research & Technology
20943 Devonshire St.
Chatsworth, CA 94588

Dennis L. Orphal

California Research & Technology, Inc.
5117 Johnson Dr.
Pleasanton, CA 94588

Mark Majerus

California Research and Technology, Inc.
PO Box 2229
Princeton, NJ 08543-2229

Mark Smith

Aerophysics Branch
Calspan Corporation/AEDC Operations
MS 440
Arnold AFB, TN 37389

G. Lyles

CIA
6219 Lavell Ct.
Springfield VA 22152

John Walton

OSWR
CIA
Washington, DC 20505

N. W. Ashcroft

Laboratory of Atomic and Solid State Physics
Clark Hall
Cornell University
Ithaca, NY 14853

Carlos Marino

Industry, Science, and Technology Department
Cray Research Park
655 E. Lone Oak Dr.
Eagan, MN 55121

Stanley Winner

David Taylor Research Center
Mail Code 3510
Bethesda, MD 20084

Major Robert Kocher

Defense Advanced Research Projects Agency
3701 North Fairfax Drive
Arlington, VA 22203-1714

R. J. Lawrence

DNA/SPSP
6801 Telegraph Rd.
Alexandria, VA 22310

Michael E. Giltrud
DNA/SPSD
6801 Telegraph Rd.
Alexandria, VA 22310

Randy Hanson
Denver Research Institute
University Park
Denver, CO 80208

Brian Scott
EI Dupont de Demours and Company
Chestnut Run - CR702
Wilmington, DL 19898

William Flis
DynaEast Corporation
3201 Arch Street
Philadelphia, PA 19104

Randall Laviolette
EG&G Idaho
P.O. Box 1625
Idaho Falls, ID 83415-2208

Tien Chou
EG&G Mound
PO Box 3000
Miamisburg, OH 45343

Julius W. Enig
Enig Associates, Inc.
11120 New Hampshire Ave., Suite 500
Silver Spring, MD 20904-2633

Kim Parnell
Failure Analysis Associates, Inc.
149 Commonwealth Ave.
P. O. Box 3015
Menlo Park, CA 94025

Vensen Wu
FMC Corporation
MS-P95
2890 De La Cruz Blvd.
Santa Clara, CA 95052

James MacDonald
General Research Corporation
PO Box 6770
Santa Barbara, CA 93160-6770

M. Goldberg, MS B44-35
Grumman Corporation
Bethpage, NY 11714

C. VanOmmersen
ICI Explosives USA, Inc.
P.O. Box 577
Tamaqua, PA 18252-0577

Guy Spitale
Jet Propulsion Laboratory
California Institute of Technology
Reliability Engineering Section
4800 Oak Grove Drive
Pasadena, CA 91109

Jeff Elder (2)
Kaman Sciences Corporation
Huntsville Office
P. O. Box 2486
Huntsville, AL 35804-2486
Attn: J. Elder, S. Jones

John May
Kaman Sciences Corporation
1500 Garden of the Gods Road
Colorado Springs, CO 80933

Thomas Grondzik
Kendall Square Research
2102 Business Center Drive, Suite 115D
Irvine, CA 92715

Kenneth Lockwood
Knolls Atomic Power Laboratory
General Electric Company
PO Box 1072
Schenectady, NY 12301-1072

E. S. Gaffney
Ktech corporation
91 1E Pennsylvania NE
Albuquerque, NM 87112

Cylinder Test Predictions Using Panda EOS

Ed Cykowski
Lockheed Engineering and Space Company
Mail Code B22
2400 NASA Road 1
Houston, TX 77058-3711

Erik Matheson (2)
0/81-12 B/157
Lockheed Missiles & Space Company
1111 Lockheed Way
Sunnyvale, CA 94088-3504
Attn: Y.-I. Choo, E. Matheson

Richard Crawford
Logicon RDA
P. O. Box 92500
Los Angeles, CA 90009

John Flowers
LTV Missiles and Electronics Group
P. O. Box 650003
M/S EM-36
Dallas, TX 75265-0003

Tim Gillespie
MS H4330
Martin Marietta Astronautics Group
PO Box 179
Denver, CO 80201

George Christoph
Martin Marietta Laboratories
1450 S. Rolling Road
Baltimore, Maryland 21227

Larry Williams
Martin Marietta
MP 126
Box 5837
Orlando, FL 32855

N. A. Louie
Department Y831, Mail Station 13-3
McDonnell Douglas Missile Space Systems
Company
5301 Bolsa Avenue
Huntington Beach, CA 92647

K Nelson
Dept. of Chemistry
MIT
77 Massachusetts Ave.
Cambridge, MA 02139

Eric Christianson
NASA Johnson Space Center
Space Science Branch/SN3
Houston, TX 77058

Scott Hill
NASA Marshall Space Flight Center
Mail Code ED52
Redstone Arsenal
Huntsville, AL 35812

John M. Pipkin (Code 4310)
Naval Coastal Systems Center
Thomas Drive
Panama City Beach, FL 32405-5000

C. T. White
Code 6179
Naval Research Lab
Washington, DC 20375-5000

Naval Surface Warfare Center (10)
10901 New Hampshire Ave.
Silver Spring, MD 20903-5000
Attn R. D. Bardo
Attn: R. R. Bernecker
Attn C. S. Coffey
Attn: J. W. Forbes
Attn: H. D. Jones
Attn H. Mair
Attn: P. Miller
Attn: D. Price
Attn: J. M. Short
Attn: D. G. Tasker

Dan Bowlus
Naval Underwater Systems Center
Mail Code 8123
Newport, RI 02841-5047

Naval Weapons Center (3)
China Lake, CA 93555-60001
Attn: A. L. Atwood, Code 3891
Attn: T. L. Boggs, Code 0239
Attn: E. Lundstrom, Code 3261

D. H. Liebenberg (2)
800 N. Quincy St.
Office of Naval Research
Arlington, VA 22217
Attn: D. Liebenberg, R. S. Miller

P.-A. Persson
CETR
New Mexico Tech
Socorro, NM 87801

Mark Walz
NMI
2229 Main Street
Concord, MA 01742

Yasuyuki Horie
Box 7908
North Carolina State University
Raleigh, NC 27695

Firooz Allahdadi (3)
Phillips Laboratory
PL/WSSD
KirtlandAFB, NM 87117-6008
Attn: F. Allahdadi, D. Fulk, D. Medina

Ray Pierce
Physics International
PO Box 5010
San Leandro, CA 94577-0599

Keith Pauley
PNL
KS-42
P. O. Box 999
Richland, WA 99352

Steve Rieco
POD Associates, Inc.
2309 Renard Place, SE
Suite 201
Albuquerque, NM 87106

C. W. Nestor, Jr.
Oak Ridge National Laboratory
PO Box 2009
Oak Ridge, TN 37831-8058

D. E. Welch
Engineering Technology Division
Oak Ridge National Laboratory
PO Box 2003
Oak Ridge, TN 37831-7294

Anthony Gurule
Orion International Inc.
Suite 200
300 San Mateo NE
Albuquerque, NM 87108

D. Matuska
Orlando Technology, Inc.
P. O. Box 855
Shalimar, FL 32579

John Remo
Quantametrics, Inc.
#1 Brackenwood Path
Head of the Harbor
St. James, NY 11780

Peter Radkowski, III
Radkowski Associates
PO Box 5474
Riverside, CA 92517-5474

Tracy Christian-Frear (10)
Re/Spec, Inc., Suite 300
4775 Indian School Rd. NE
Albuquerque, NM 87110

Greg L. Savoni
Rockwell International Corporation
12214 Lakewood Blvd.
NA-40
Downey, CA 90241

R&D Associates
6053 West Century Boulevard
P.O. Box 92500
Los Angeles, CA 90009
Attn: B. Lee

Cylinder Test Predictions Using Panda EOS

Mark Fry
SAIC/New York
8 West 40th Street
14 Floor
New York, New York 10018

Ronald Weitz
SAIC
2109 Air Park Road SE
Albuquerque, NM 87106

James Zerkle
SAIC, M/S C-2
10260 Campus Point Drive
San Diego, CA 92121

Charles E. Needham
Maxwell/S-CUBED
2501 Yale SE
Suite 300
Albuquerque, NM 87106

Steve Peyton
S-CUBED
P. O. Box 1620
LaJolla, CA 92038-1620

C. E. Anderson (2)
Southwest Research Institute
P.O. Drawer 28510
San Antonio, TX 78284
Attn.: C. E. Anderson, J. D. Walker

William G. Tanner
Space Science Laboratory
P. O. Box 97303
Waco, TX 76798

M. Cowperthwaite
SRI International
333 Ravenswook Ave.
Menlo Park, CA 94025

L. Seaman
SRI International
333 Ravenswook Ave.
Menlo Park, CA 94025

Bhuminder Singh (2)
Teledyne Brown Engineering
Cummings Research Park
300 Sparkman Dr., NW
PO Box 070007
Huntsville, AL 35807-7007
Attn: B. Singh, B. Loper

Steve Herrick
Textron Defense Systems
Mail Stop 1115
201 Lowell St.
Wilmington, MA 01887

Dwight Clark, Mailstop 280
Thiokol Corporation
Advanced Technology Division
P. O. Box 707
Brigham City, Utah 84302

Akhilesh Maewal
Trans-Science Corporation
7777 Fay Avenue
Suite 112
La Jolla, CA 92037

Stan Fink, R1/1044
TRw
One Space Park
Redondo Beach, CA 90278

T. P. Shivananda
TRW Ballistic Missiles Group
SB/2/1011
P. O. Box 1310
San Bernardino, CA 92402-1310

Brent Webb
Umpqua Research Company
P. O. Box 791
125 Volunteer Way
Myrtle Creek, OR 97457

Gene Carden
University of Alabama
PO Box 870278
Tuscaloosa, AL 35487-0278

Gary Hough
Aerophysics Research Facility
University of Alabama at Huntsville
Huntsville, AL 35899

R. Jeanloz
Department of Geology and Geophysics
University of California
Berkeley, CA 94720

David J. Benson
Dept. of AMES R-011
University of California San Diego
La Jolla, CA 92093

Robert Culp
Department of Aerospace Engineering
Sciences
Campus Box 429
University of Colorado
Boulder, CO 80309

Garry Abfalter
Impact Physics Group
University of Dayton Research Institute
300 College Park, Room KLA 14
Dayton, OH 45469-0182

G. Ali Mansoori
Department of Energy Engineering
University of Illinois at Chicago Circle
Box 4348
Chicago, IL 60680

Chen-Chi Hsu
University of Florida
Department of Aerospace Engineering
231 Aerospace Building
Gainesville, FL 32611

Murli H. Manghnani
Hawaii Institute of Geophysics
University of Hawaii
Honolulu, Hawaii 96822

Scott Stewart
Department of Theoretical and Applied
Mechanics
University of Illinois
Urbana, Illinois 61801

R.W. Armstrong
Department of Mechanical Engineering
University of Maryland
College Park, MD 20742

R. D. Dick
Department of Mechanical Engineering
University of Maryland
College Park, MD 20742

R. L. McCrory
Laboratory for Laser Energetic
University of Rochester
250 East River Road
Rochester, NY 14623-1299

H. M. Van Horn
Department of Physics and Astronomy
University of Rochester
Rochester, NY 14627

Thomas Moriaty
Department of Engineering Sciences and
Mechanics
University of Tennessee
Knoxville, TN 37996-2030

Stephan J. Bless
The University of Texas at Austin
Institute for Advanced Technology
4030-2 W. Braker Lane, Suite 200
Austin, TX 78712

Eric Fahrenthold
Dept. of Mech. Engineering
The University of Texas at Austin
Austin, TX 78712

R. A. Schapery
Dept. of Aerospace Engineering
The University of Texas at Austin
Austin, TX 78712

Chadee Persad
Institute for Advanced Technology
The University of Texas at Austin
4030-2 W. Braker Ln.
Austin, TX 78759-5329

Cylinder Test Predictions Using Panda EOS

Keith Holsapple

Department of Aeronautics and Astronautics
FS10
The University of Washington
Seattle, WA 98195

S. A. Schakelford

FJSRL/NC (AFSC)
USAF Academy, CO 80840-6528

Y. M. Gupta

Department of Physics
Shock Dynamics Laboratory
Washington State University
Pullman, WA 99164-2814

Wright Laboratory (5)

Eglin AFB, FL 32542-5434

Attn: D. Brubaker

Attn: J. A. Collins

Attn: J. Foster

Attn: R. L. McKenney

Attn: B. Patterson

J. M. McBride

Dept. of Chemistry
Yale University
P.O. Box 6666
New Haven, CT

J. H. S. Lee

Dept. of Mech. Engineering
McGill University
Montreal, Quebec
CANADA H3A 2K6

A. Ng

Department of Physics
University of British Columbia
Vancouver, BC V6T 26A
CANADA

J. Boileau

Societe Nationale des Poudres et Explosifs
12 Quai Henri IV
75004 Paris
FRANCE

R. Cherét

Commissariats à l'Energie Atomique 33
Rue de la Federation
Paris, 75015
FRANCE

Centre d'Etudes de Limeil-Valenton (2)

Attn: F. Perrot, M. Penicaud

B.P. 27

F-94190 Villeneuve St. Georges

FRANCE

Centre d'Etudes de Vaujours (4)

Attn: R. Chirat, J. Baute, J. M. Chevalier, L Brun

B.P. 7

F-7718 1 Courtry

FRANCE

D. Bergues

Commissariats à l'Energie Atomique
Centre de'Etudes de Gramat
Gramat, 46500
FRANCE

H. N. Presles

ENSMA

Laboratoire d'Energétique et de Détonique

Poitiers (Cedex) 86034

FRANCE

J.-P. Hansen

Ecole Normale Supérieure de Lyon

46, allée d'Italie

69364 Lyon Cedex 07

FRANCE

H. Moulard/M. Samirant

Institut Saint Louis

5, rue de l'Industrie

BP 3468301

Saint Louis

FRANCE

M. Held

MBB Schrobhausen

D-8898 Schrobhausen

GERMANY

F. Hensel
Fachbereich Physikalische Chemie
Philipps-Universität Marburg
Hans-Meerwein-Strasse
 D-3550 Marburg
 GERMANY

V. Hohler
Ernst-Mach-Institut
Eckerstrasse 4
 7800 Freiburg i.BR
 GERMANY

F. Volk
Fraunhofer-Institut für Chemische Technology
 D-7507 Pfinztal-Berghausen
 GERMANY

S. K. Sikka
 High Pressure Physics Division
Bhabha Atomic Research Centre
 Trombay, Bombay -400085
 INDIA

Y. Rosenfeld
 Nuclear Research Center - Negev
 P.O. Box 9001
 Beer Sheva
 ISRAEL

K. Tanaka
 National Chemical Lab for Industry
 Explosives Chemistry Section
Tsukuba Ibaraki 305
 JAPAN

T. Hikita
Fukui Institute of Technolgy
Gakuen, Fukui 910
 JAPAN

Y. Kato
 Chemicals and Explosives Laboratory
 Nippon Oil and Fats Co., Ltd.
 Taketoyo, Aichi 470-23
 JAPAN

G. A. Leiper
 ICI Explosives
 Stevenston, Ayrshire
 SCOTLAND

Fernando Alcalde
 Union Espanola De Explosives
Claudio Coello, 124
 Madrid, 28006
 SPAIN

J. Campos/J. C. Gois
S.A. Eng. Mecanica
 Fat. of Science and Technology
 University of **Coimbra**
 3000 **Coimbru**
 PORTUGAL

A. N. Dremin
 Institute of Chemical Physics
 Chemogolovka, **P.O. 142432**
 Moscow region, RUSSIA

V. I. Fortov
 Institute of Chemical Physics
Chernogolovka, P.O. 142432
 Moscow region, RUSSIA

I. V. Lomonosov
 Institute of Chemical Physics
Chernogolovka, P.O. 142432
 Moscow region, RUSSIA

H. Ostmark
 FOA Section 243
 17290 Sundbyberg
 SWEDEN

M. COOUP. Haskins
 Defence Research Agency
 Sevenoaks, Kent
 UNITED KINGDOM

J. E. Field/M. M. Chaudhri
 Dept. of Physics
 University of Cambridge
Cavendish Laboratory, Madingley Road
 Cambridge CB3 0HE
 UNITED KINGDOM

Cylinder Test Predictions Using Panda EOS

B. D. Lambourn
Atomic Weapons Establishment
Aldermaston, Reading, RG74PR
Berkshire
UNITED KINGDOM

W. Byers Brown
University of Manchester
Department of Chemistry
Manchester, M13 9PL
UNITED KINGDOM

Los Alamos National Laboratory (72)
Mail Station 5000
P.O. Box 1663
Los Alamos, NM 87545

Attn: J. Abdallah, MS-2 12
Attn: T. F. Adams, MS F663
Attn: B. I. Bemett, MS B221
Attn: S. T. Bennion, MS F663
Attn: J. B. Bdzil, MS P952
Attn: W. Birchler, MS G787
Attn: P. J. Blewett, MS F663
Attn: R. J. Bos, P-5
Attn: M. W. Burkett, MS G787
Attn: E. J. Chapyak, MS F663
Attn: R. A. Clark, MS B257
Attn: G. E. Cort, MS G787
Attn: C. W. Cranfill, MS-B257
Attn: B. J. Daly, MS B216
Attn: W. C. Davis, MS-P952
Attn: T. N. Dey, MS-F665
Attn: J. J. Dick, MS-P952
Attn: J. K. Dienes, MS B216
Attn: H. Flaush, MS C936
Attn: C. A. Forest, MS-P952
Attn: R. P. Godwin, MS F663
Attn: F. Harlow, MS B216
Attn: W. B. Harvey, MS F663
Attn: B. L. Holian, MS J569
Attn: K. S. Holian, MS B295
Attn: J. W. Hopson, MS B216
Attn: H. Horak, MS C936
Attn: M. L. Hudson, MS J970
Attn: E. S. Idar, MS-J960
Attn: J. D. Johnson, MS-B221
Attn: J. N. Johnson, MS-B221
Attn: N. L. Johnson, MS B216

Attn: J. E. Kennedy, MS-B950
Attn: J. F. Kerrisk, MS G787
Attn: M. Klein, MS F669
Attn: D. Kothe, MS-B216
Attn: R. A. Krajcik, MS-F218
Attn: W. H. Lee, MS B226
Attn: R. A. Lesar, MS-B262
Attn: L. B. Luck, MS-K557
Attn: C. L. Mader, MS-B214
Attn: J. M. Mack, MS-P940
Attn: D. Mandell, MS F663
Attn: L. G. Margolin, MS D406
Attn: G. H. McCall, MS B218
Attn: J. K. Meier, MS G787
Attn: R. W. Meier, MS G787
Attn: A. L. Merts, MS-212
Attn: C. E. Morris, MS-J970
Attn: T. R. Neal, MS-P940
Attn: A. T. Oyer, MS G787
Attn: D. A. Poling, MS-F669
Attn: C. E. Ragan, MS-D449
Attn: J. Ramsay, MS-J960
Attn: M. Rich, MS F669
Attn: J. P. Ritchie, MS-B214
Attn: M. Sahota, MS B257
Attn: G. L. Schott, MS P952
Attn: B. P. Shafer, MS-K574
Attn: J. W. Shaner, MS-J970
Attn: D. H. Sharp, MS-B285
Attn: S. Shaw, MS-B214
Attn: S. A. Sheffield, MS-P952
Attn: W. Sparks, MS F663
Attn: C.B. Storm, P915
Attn: G. K. Straub, MS-B221
Attn: P. K. Tang, MS-F664
Attn: M. T. Thieme, MS-F664
Attn: D. Tonks, MSB221
Attn: H. E. Trease, MS B257
Attn: J. D. Wackerle, MS-P952
Attn: L. Witt, MS C936

University of California(31)
Lawrence Livermore National Laboratory
7000 East Ave.
P.O. Box 808
Livermore, CA 94550

Attn: A. Attia, L-200
Attn: D. E. Burton, L-18
Attn: R. B. Christensen, L-35
Attn: G. R. Gathers, L368
Attn: H. C. Graboske, L-296
Attn: L. G. Green, L-282
Attn: R. Grover, L-299
Attn: J. W. Kury, L-368
Attn: J. M. LeBlanc, L-35
Attn: E. L. Lee, L-368
Attn: D. A. Liberman, L-477
Attn: A. K. McMahan, L-299
Attn: W. Moran, L-200
Attn: R. M. More, L-321
Attn: M. J. Murphy, L-368
Attn W. J. Nellis, L-299
Attn: A. L. Nichols, L-368
Attn: W. Quirk, L-35
Attn: J. E. Reaugh, L-290
Attn: F. H. Ree, L-299
Attn: C. E. Rosenkilde, L-84
Attn: M. Ross, L-299
Attn: R. L. Simpson, L-282
Attn: P. C. Souers, L-368
Attn: D. J. Steinberg, L-35
Attn: W. C. Tao, L-282
Attn: C. M. Tarver, L-368
Attn: R. E. Tipton, L-35
Attn: M. van Thiel, L-299
Attn: M. Wilkins, L-321
Attn: D. A. Young, L-299

Internal Distribution

1153 G. A. Samara
1153 R. A. Graham
1153 A. C. Switendick
1241 M. A. Sweeney
1271 M. K. Matzen
1271 G. O. Allshouse
1271 E. J. McGuire
1400 E. H. Barsis
1402 S. S. Dosanjh
1404 J. A. Ang
1408 J. N. Jortner
1415 G. S. Davidson
1421 W. J. Camp
1422 R. Allen
1423 E. F. Brickell
1424 A. L. Hale
1425 J. H. Biffle
1431 J. M. McGlaun
1431 K. G. Budge
1431 M. G. Elrick
1431 E. S. Hertel
1431 J. S. Peery
1431 S. V. Petney
1431 A. C. Robinson
1431 T. G. Trucano
1431 M. Wong
1431 CTH Day File
1432 P. Barrington
1432 R. L. Bell
1432 R. M. Brannon
1432 P. J. Chen
1432 H. E. Fang
1432 A. V. Farnsworth
1432 G. I. Kerley (10)
1432 M. E. Kipp
1432 F. R. Norwood
1432 S. A. Silling
1432 P. A. Taylor
1433 P. L. Stanton
1433 M. Boslough
1433 D. A. Crawford
1433 L.C. Chhabildas
1433 M. D. Furnish
1433 D. E. Grady
1434 D. Martinez
1511 J. S. Rottler
1512 A. C. Ratzel

Cylinder Test Predictions Using Panda EOS

1512 M. R. Baer
1512 M. L. Hobbs
1513 R. D. **Skocypec**
1553 W. L. **Hermira**
1561 H. S. Morgan
1562 R. K. Thomas
2512 J. G. Harlan
2513 D. E. Mitchell
2513 S. G. **Barnhart**
2513 S. H. Fischer
2513 S. M. **Harris**
2513 M. G. **Vigil**
2514 L. L. Bonzon
2514 A.M. **Renlund**
2514 L. J. **Weirick**
5166 R. E. **Setchell**
5602 J. R. Asay
6111 J. L. Wise
6117 W. R. Wawersik
6119 R. W. **Ostensen**
6418 S. L. **Thompson**
6418 L. N. Kmetyk
6515 M. Berman
6515 K Boyack
8741 G. A. **Benedetti**
8741 M. L. **Chiesa**
8741 L. E. **Voelker**
8742 J. J. Dike
8243 M. L. **Callabresi**
8743 D. J. **Bammann**
8745 R. J. Kee
9311 A. J. **Chabai**
9311 T. **Bergstresser**
9333 P. W. Cooper
9702 T. **Hitchcock**
9722 R. O. **Nellums**
9723 J. M. **Holovka**
9723 M. J. **Forrestal**
8523-2 Central Technical Files
7141 **Technical Library** (5)
7151 **Technical Publications**
7613-2 Document Processing for DOE/OSTI
(10)